Growth of metallic nanowires by chemical etching and the use of Microfluidics channels to produce quantum point contacts

by

Fatemeh Soltani
B.Sc., Iran University of Science and Technology, 2006

A Thesis Submitted in Partial Fulfillment
of the Requirements for the Degree of

MASTER OF SCIENCE

in the Department of Physics and Astronomy

Supervisory Committee

Growth of metallic nanowires by chemical etching and the use of Microfluidics channels to produce quantum point contacts

by

Fatemeh Soltani
B.Sc., Iran University of Science and Technology, 2006

Supervisory Committee

Dr. Geoffrey Steeves (Supervisor)

Department of Physics and Astronomy

Dr. Byoung-Chul Choi (Departmental Member)

Department of Physics and Astronomy

Dr. Andrew Jirasek (Departmental Member)

Department of Physics and Astronomy

Abstract

Supervisory Committee

Dr. Geoffrey Steeves (Supervisor)

Department of Physics and Astronomy

Dr. Byoung-Chul Choi (Departmental Member)

Department of Physics and Astronomy

Dr. Andrew Jirasek (Departmental Member)

Department of Physics and Astronomy

A self-terminated electrochemical method was used to fabricate microscopic-scale contacts between two Au electrodes in a microfluidic channel. The conductance of contacts varies in a stepwise fashion showing quantization near the integer multiples of the conductance quantum (G_0). The mechanism works by a pressure-driven flow parallel to a pair of Au

electrodes with a gap on the order of micron in an electrolyte of HCl. When applying a bias voltage between two electrodes, metal atoms are etched off the anode and dissolved into the electrolyte as metal ions, which are then deposited onto the cathode. Consequently, the gap decreases to the atomic scale and then completely closes as the two electrodes form a contact. The electrochemical fabrication approach introduces large variance in the formation and location of individual junctions. Understanding and controlling this process will enable the precise positioning of reproducible geometries into nano-electronic devices.

Table of Contents

List of Figures

List of tables

Acknowledgments

Funding support from the Natural Sciences and Engineering Research Council of Canada (NSERC) and the University of Victoria has enabled the project's completion.

Contributions from my colleague Alex Wlasenko and helpful assistant of students in the Microfluidics lab of Mechanical Engineering have been important during various phases of the project.

The technical staff at the University of Victoria including electronics technicians Nicolas Braam, Mike Pfleger and Niel Honkanen as well as machinist David Smith and Chris Secord have been invaluable sources of expertise. Their assistance has been greatly appreciated.

The faculty and staff at the University of Victoria especially Dr. David Sinton has provided helpful input and shared necessary equipment.

Lastly I offer my sincerest gratitude to my supervisor, Dr. Geoffrey Steeves, who has supported me throughout my thesis with his patience and knowledge that allowed me to work in my own way. I am so thankful to his encouragement and effort. His continued support in terms of technical advice and resources has made this project possible.

Dedication

To my Mom and my Dad,

Who always provide me with their best efforts. Their love and support are my wings to fly toward future and achieve my dreams. None of these would have been possible without your encouragements.

Thank you!

Chapter 1

Introduction

The goal of this work is to study some of the properties of quantum point contacts (QPC). There will be discussions on what they are, why they are important and how they can be fabricated. Then a new technique for fabrication will be introduced which consists of electrochemically etched metallic electrodes and making connections by electro-deposition in microfluidic channels. There are several ways that these devices are characterised that made by the technique, including analyzing Scanning Electron Microscopy (SEM) micrographs, modeling the growth of quantum point contacts and different electrical methods. Motivation for accomplishing this work will be to study of point contacts' dynamics. Ongoing research on Direct Current (DC) transport and ultrafast electrical displacement measurement techniques, like time-resolved Scanning Tunnelling Microscope (STM), are some of our main interests.

1.1 General discussions and requirements

For understanding properties of microfabrication it is important to consider some of the main concepts. Discussion about dynamics behaviour of electrons in small dimensions will follow topics of this section.

1.1.1 Mean free path: Charge transport has been used to characterize many different physical devices. If a wire has been taken and be pulled until it gets sufficiently thin to become one-dimensional, a mechanical break junction can be formed. This will be thin enough to compare with microscopic physical parameters such as electron mean free path and Fermi wavelength. The mean free path is the average distance covered by an electron to move freely before collision with other electrons in subsequent impacts. The mean free path (l) could be taken as the length of the path divided by the number of collisions. For example in a cylindrical shape wire with cross section radius of r:

Mean free path estimate = (distance traveled by electron) / [(volume of interaction) * (number of electrons per volume)]

$$l = \frac{\bar{v}t}{\pi r^2 \bar{v}t \times n_e} = \frac{1}{\pi r^2 n_e} \qquad (1.1)$$

where $\bar{v}$ is average velocity of electrons and n_e is number of electrons per volume. Also t is the time that electron travels in the defined distance and r is the radius of circular cross section.

The mean free path (m.f.p.) of electrons in semiconductors can be made as long as tens of μm $(\sim 10^{-5} m)$ at low temperatures (by adding dopants) and the m.f.p. of the electrons are hundreds of nm $(\sim 10^{-7} m)$. The m.f.p. of the conduction electrons for most metals is only a few Å.

1.1.2 Ballistic transport: The entire path that an electron travels freely without collision is considered as ballistic transport. In a nanowire, ballistic transport should be considered as the transport of electrons in a medium with negligible electrical resistivity due to scattering. Without scattering, electrons simply obey Newton's first law of motion (at non-relativistic speeds) and try

to maintain their preliminary speed and direction. The story of ballistic transport goes back to 1965, when Yuri Sharvin used a pair of point contacts to demonstrate ballistic transport over opening distance of about 10 nm [1], to inject and detect a beam of electrons in a metallic single crystal. In such experiments, the quantum mechanical wave character of the electrons does not play an essential role, because the order of its wavelength ($\lambda_F \approx 0.5$ nm) is much smaller than the opening of the point contact [2].

1.1.3 Fermi wavelength: When we discuss the eigenstates of the electrons, the Fermi wavelength becomes relevant. Usually Fermi wavelength is illustrated by referring to the energy of the highest occupied quantum state in a system of fermions (like electrons in a metal). It mostly appears at very low temperatures. If the electrons are confined in a box, quantum mechanics tells us that the electrons can have only discrete values of kinetic energy. The energetic spacing of the eigenvalues depends on the dimensions of the box. However the smaller the box, the larger the spacing is. [4]

$$\Delta E_L = \frac{h^2}{2m(\pi / L)^2} \qquad (1.2)$$

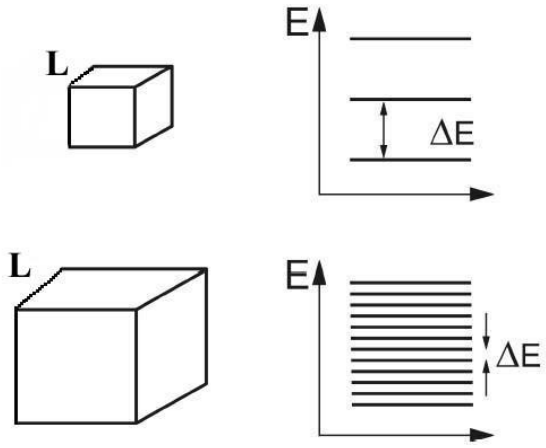

Figure 1.1 - Energy levels in a box

Where ΔE_L is the spacing and "L" is the length of the box. The Fermi level is the highest occupied state (at absolute zero). The wavelength of electrons at the Fermi level is known as the Fermi wavelength. If the size of the box is just the Fermi wavelength; only the first eigenstates are occupied. A thin wire is like a small box for electronic motion perpendicular to the wire's axis.

1.1.4 Classical resistance: In the conventional view, the electrical resistance of an object is a measure of its opposition to the passage of a steady electrical current. Conduction electrons experience multiple diffusive scattering when they travel through a wire. An object of uniform cross section will have a resistance proportional to its length and inversely proportional to its cross-sectional area, and proportional to the resistivity of the material (ρ).

$$R = \rho \frac{l}{A} \quad (1.3)$$

The length of wire deals with mean free path concept of transport and width of wire is important when we want to consider low dimensions and talk about Fermi wavelength. (Fig. 1.2) [5]

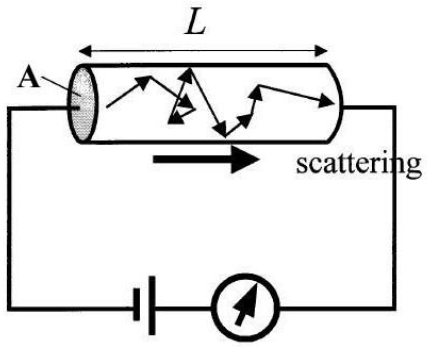

Figure 1.2- Classical scattering

1.1.5 Quantum resistance: As materials or devices shrink from ordinary scales down to the nanoscale, interesting quantum effects happen. In the quantum view, concepts of classical electronic transport such as conduction or resistivity have been changed. Conceptually, the simplest of these nanoscale solid-state devices is the ballistic one-dimensional wire, in which the transverse motion has been quantized into discrete modes, and the longitudinal motion is free. The length is decreasing below the electron mean free path and the diameter of the wire is shrunk to the order of the electron Fermi wavelength (Fig. 1.3) [5]. In this case electrons are envisioned to propagate freely down a clean narrow pipe (without any electron collisions). However, the actual resistance of such a wire is found to be very different from zero. Instead, its value is the resistance quantum ($R_0 = h/2e^2$) divided by the number of occupied transverse modes. Hence, in the quantum limit, when the pipe is sufficiently narrow to support only a single mode, the resistance of a perfect wire is rather large: $R_0 \approx 12.9 \approx 13$ kΩ. [6]

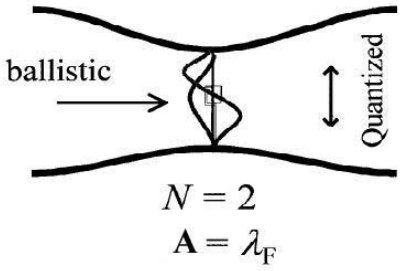

Figure 1.3 – Waveguide in a metallic nano wire

where A is the cross section of the thin wire.

1.1.6 Two-Dimensional Electron Gas (Two-DEG) structure: In a metal, a point contact is fabricated simply by pulling a wire from its sides. But in a semiconductor forming a quantum point contact mostly requires a more complicated strategy. The two – dimensional electron gas in a GaAs – AlGaAs heterojunction has two important properties. First is its Fermi wavelength which is hundred times larger than in a metal (The Fermi wavelength of metal is typically in order of Å [2] and Fermi wavelength of electrons in a 2DEG is about tens of nm [7]). This makes it possible to study a constriction with an opening comparable to the wavelength. Second is that by using this wavelength which is much smaller than the mean free path for impurity scattering, usual defects in confined structures are avoidable. Such a constriction forms a quantum point contact between two wide electrically – conducting regions, of a width (is in the order of μm in 2DEG) [10], where the size of the junction is of similar dimension to the wavelength of the electron. The transverse confinement in the quantum point contact results in a quantization of the transverse motion much like in a waveguide. Formation and theory of 2DEG structures will be mentioned in detail in the theory of QPC section (1.3).

1.2 Experimental Observations of Quantized Conductance

As historical review, there was the debate [2] whether a wire without impurities could have any resistance at all. Ultimately, the question was: "What is measured when you measure a resistance?" The conventional point of view is that conduction would be the flow of current in response to an electric field which was supported by classical Drude-Sommerfeld theory. It is about the linear dependence of current density and electric field.

$$J = \left(\frac{nq^2\tau}{m} \right) E \qquad (1.4)$$

where τ is mean free path time between collisions and n is number density. Also q, m are electron charge and electron mass respectively. The term in parenthesis was measured as related resistance. An alternative point of view was proposed by Landauer (1957) who was mentioning in a quantum view that current is the flow of independent and degenerate electrons as they follow a nominal density gradient across reservoirs, and conductance is without loss transmission through an interposed quantum barrier. Because of the experimental implication in that time, result of debate remained unclear until recent years.

When experiments began to investigate properties of QPCs, one of the first important effects was the search for a quantum size effect on the conductance, which would reveal clearly the one dimensional density of states of electrons confined to a narrow wire [11]. The density of states (DOS) of a system describes the number of states at each energy level that are available to be occupied. In narrow wires, as a quantization effect, the DOS for certain energies actually becomes higher than the DOS for bulk semiconductors. This phenomenon is apparent at the

Fermi wavelength. For a perfect conductance, the electron motion should be ballistic at Fermi energy.

As a good example, it has been observed in the case of GaAs / AlGaAs heterostructure devices, increasing the width of the opening by varying the voltage on the gate electrode makes conductance increase stepwise as a function of width of point contact or gate. The bigger the opening, the bigger the current. The special property of the quantum point contact is upon widening the opening; the current does not increase gradually but stepwise [15]. In principle, the authors [16] observed that the nature of each step is like a staircase in conductance by value of $\frac{2e^2}{h}$ as anticipated. Experimental data has been showed in the figure below, these steps are obvious in the B=0 curve.

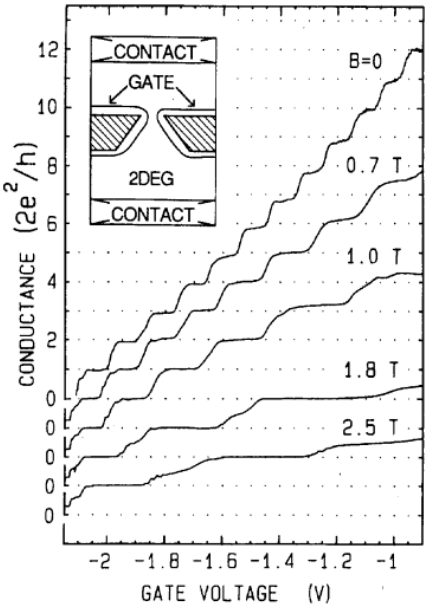

Figure 1.4- Steps of conductance in 2DEG

Discussion about step-shape changes corresponding to magnetic field variations is not in the scope of this research. But just as a hint for interested readers, an external magnetic field applied to the quantum point contact lifts the spin degeneracy so the number N of modes that contribute becomes smaller.

1.3 The theory of Quantum Point Contacts

If $I = GV$ is resembling Ohm's law for macroscopic resistors (G is showing conductance here), then if we assume the case that under the condition that voltage remains unchangeable, the stepwise increase of conductance will be obvious. As a result quantization of conductance is observable. This means that conductance cannot vary continuously and must be discrete multiples of elementary value of quantum conductance (G_0).

$$G = N \times \frac{2e^2}{h} \longrightarrow G_0 = \frac{2e^2}{h} \qquad (1.5)$$

($\frac{2e^2}{h}$) is quantum of conductance and equals to resistance of 12.9 k Ω

(N) is the closest integer to the ratio of multiples of quantum conductance. It is also the width of the contact divided by half of the electron wavelength. The electron wave can only pass through the hole in one of the few resonant modes of vibration, for which the interference is constructive rather than destructive. The number (N) counts the number of modes with constructive interference.

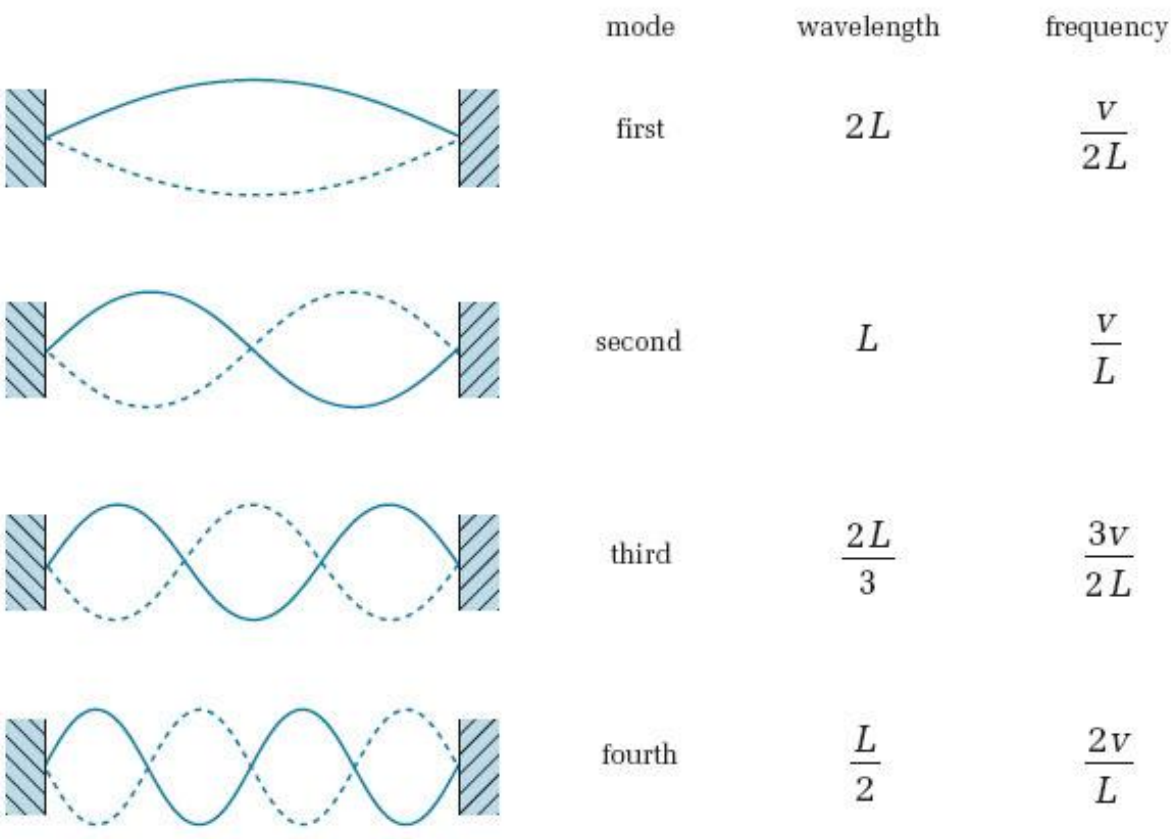

Figure 1.5- Modes of a standing wave

As a result of high mobility (85 $\frac{m^2}{V}$) attainable in the two-dimensional electron gas in GaAs-AlGaAs heterostructures (ability to move for carriers in 2DEG), it is feasible to study ballistic transport in small devices [17]. The resistance is determined by the point-contact geometry only. The point contacts are defined by electrostatic depletion of the 2DEG underneath a gate. Whereas control of the width is not feasible in metal point contacts, it is controllable in the 2DEG, this method offers possibility to control the width of the point contact by the gate voltage. The gate is a negatively charged electrode on top of the heterostructure, which depletes the electron gas beneath it [2]. The picture below is a Schematic cross-sectional view of a

quantum point contact, defined in a high-mobility 2D electron gas at the interface of a GaAs-AlGaAs heterojunction.

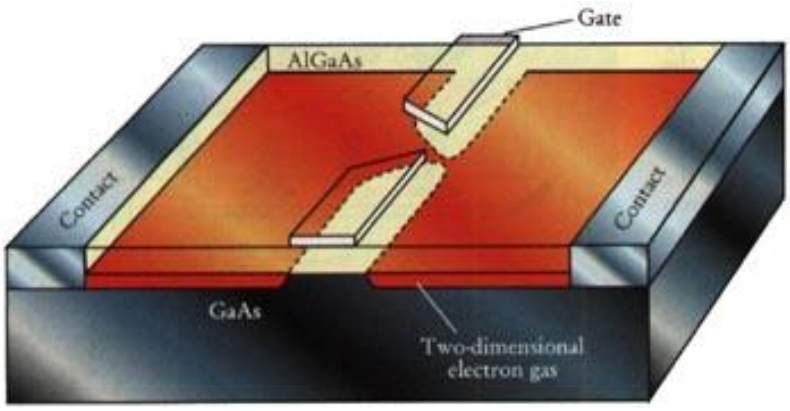

Figure 1.6 – Experimental set up of a 2DEG [2]

An elementary explanation of the quantization views the constriction as an electron wave guide, through which a small integer number $N \approx 2W/\lambda_F$ of transverse modes can propagate at the Fermi level (W is width of the gap). The wide regions at opposite sides of the constriction are reservoirs of electrons in local equilibrium. A voltage difference (V) between the reservoirs includes a current (I) through the constriction, equally distributed among (N) modes. This equipartition rule is not immediately obvious, because electrons at the Fermi level in each mode have different group velocities v_n. However, the difference in group velocity is cancelled by the difference in the density of states $\rho_n = \frac{1}{v_n h}$.

As a result, each mode carries the same current of $I_n = Ve^2\rho_n$, $v_n = \frac{V}{e^2 h}$ (1.6)

Summing over all modes in the waveguide, one obtains the conductance $G = \frac{I}{V} = \frac{Ne^2}{h}$. The experimental step size is twice $\frac{e^2}{h}$ because spin – up and spin – down modes are degenerate.

The electron waveguide has a non-zero resistance even though there are no impurities, because of the reflections occurring when a small number of propagating modes in the wave guide is matched to a larger number of modes in the reservoirs.

Figure below shows conductance quantization of a quantum point contact in units of $\frac{2e^2}{h}$. As the gate voltage defining the constriction is made less negative, the width of the point contact increases continuously, but the number of propagating modes at the Fermi level increases stepwise. The resulting conductance steps are smeared out when the thermal energy becomes comparable to the energy separation of the modes.

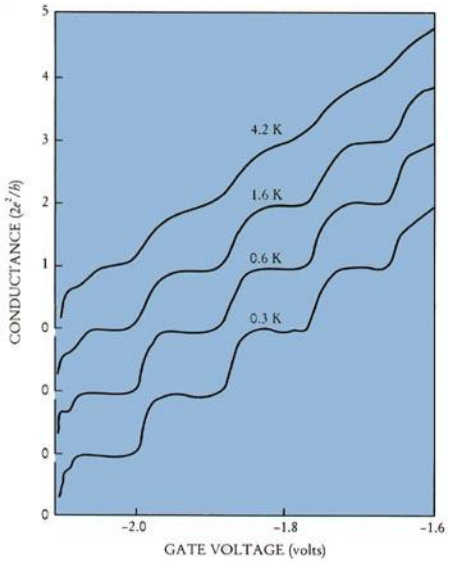

Figure 1.7 – Steps of conductance in 2DEG by temperature [2]

1.4 Conclusions

A quantum point contact is a narrow constriction between two wide electrically-conducting regions, of a width comparable to the electronic wave length. In a metal, the Fermi wavelength is the same order as atomic separation, so a QPC is necessarily of atomic dimensions. Upon making contact the conductance jumps in order of quantum conductance ($\frac{2e^2}{h}$) as the contact area is increased.

Apart from studying fundamentals of charge transport in mesoscopic conductors, quantum point contacts can be used as extremely sensitive charge detectors. Since the conductance through the contact strongly depends on the size of constriction, any potential fluctuation in the vicinity will influence the current through the QPC.

There are many ways to make QPCs which will be explained in next chapter. The most important one that we will emphasis on this research is electrochemically fabrication of metallic contacts. These contacts are called metallic nanowires. The width of nanowires can be controlled flexibly by etching atoms away or depositing atoms back onto the wire with the electrochemical potential.

There is a good method by Boussaad and Tao [18] describing how to fabricate atomic-size contacts. They used different gap voltages and record data on conductance corresponding to time. Also they got I-V curves showing stepwise staircase as expected in quantum scales. Their demonstration is a good evidence of quantized conductance. Its changes by verification in experiment's condition are so sensitive.

Chapter 2

In this chapter some of main fabrication techniques that have been used to make QPCs will be discussed. The following section includes a new approach of electrochemically etched electrodes and origin of it. At the last part we will discuss some of theoretical concepts.

2.1 Fabrication Techniques

Fabrication of QPC is an important and sensitive issue. Usually it has been done in three main ways:

2.1.1 Mechanical break junction: Mechanical confinement deals with pulling apart a piece of conductor until it breaks. The pulling causes the metal wire to break in a controlled manner to a precision of angstroms. The breaking point forms the point contact. As the electrodes are pulled apart, numbers of metallic single atoms try to bridge between the two electrodes. The process is controlled by measurement of the current flow across the metal. Each strand has a conductance equal to quantum of conductance (G_0). As the wire is pulled, the neck becomes thinner with fewer atomic strands in it. Each time the neck reconfigures, a step-like decrease of the conductance can be observed.

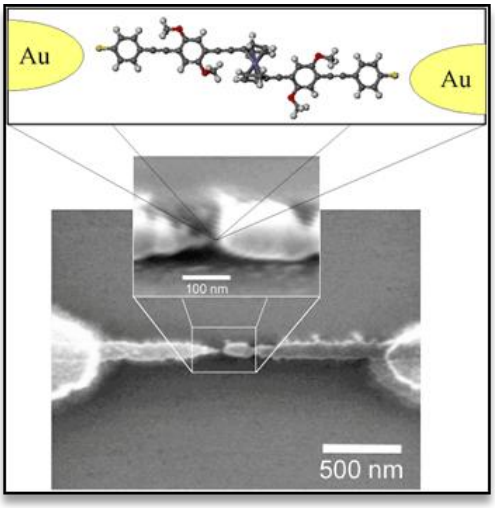

Figure 2.1- Mechanically break junction in Au [19]

Benefits of this method are that nanowires can be produced quickly and reproducibly. Disadvantages are that by pushing together or pulling away two electrodes, the length and cross section of the wires are changing. The pushing or pulling processes involve mechanical instability and guide to successive abrupt rearrangements of the atoms in the wires, which are reflected in jumps in the plots of conductance [20]. It is important to mention that also these contacts are not robust.

2.1.2 Two-DEG heterostructures: Two-DEG construction is a more controlled way which by applying a voltage to suitably – shaped gate electrodes on top of electron gas and in the appropriate edges , the electron gas can be locally depleted and many different types of conducting regions can be created in the plane of the 2DEG as quantum point contacts. (Figure 1.6)

This method was first clearly demonstrated in semiconductor devices containing 2DEG at low temperature [5]. Because of long mean free path of electrons (tens of μm, 10^{-5}), rather than wavelength of electrons (hundreds of nm, 10^{-7}). Devices that exhibit the quantum phenomenon can be fabricated with microfabrication techniques based on optical and electron beam lithography. Difficulties of this method can be mentioned as complicated procedure to make this structure. Also it is not possible to scan the non metallic surface by STM.

2.1.3 STM tip structure: STM-tip connection is made by positioning an STM tip close to the surface of a conductor. This method has the potential of forming atomic contacts to get fast response time [20]. The tip, which is mounted on a STM head, is driven towards a metallic

substrate (sample) until tunnelling current is achieved. The electrode is then withdrawn from the substrate and held at distance. By applying a large voltage it is possible to control the potential between these two junctions, deposition starts predominantly from the tip and grows toward the substrate. Therefore, the rise and fall in the conductance can be controlled by the potentials.

In contrast to mechanically break junctions, advantages of this method can be mentioned as the length of the constriction in the present system is fixed by the separation of the tip and substrate. Therefore, the stepwise change in the conductance comes from the change in the cross section of the nanowires [20]. This method also has several disadvantages: first, it takes long-term stability, which is not desirable for applications and measurements. Second, the STM is expensive and bulky. Finally, the STM setup can fabricate only one nanowire at a time.

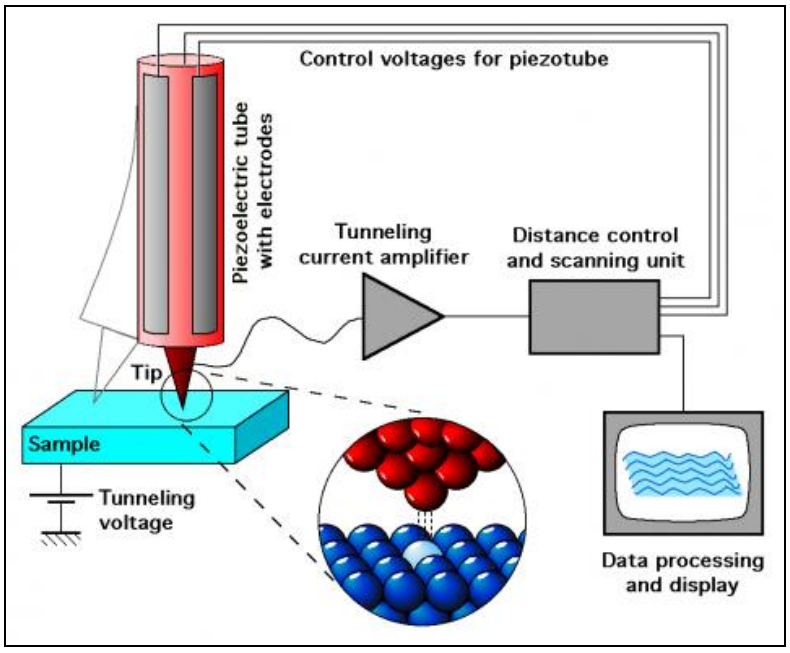

Figure 2.2- STM tip as QPC [6]

2.1.4 Proposed technique of electrochemically etched QPCs: Comparable to the size of an atom, the wavelength of the conduction electrons for most metals is only a few Å. So metallic nanowires with conductance quantized at the lowest steps must be atomically thin. Such small metallic wires cannot be easily fabricated by conventional fabrication techniques. But since the energy separation of quantum modes in metallic nanowires is large, conductance quantization is visible even at room temperature [5]. The width of the nanowires can be controlled flexibly by etching atoms away or repositioning atoms back onto the wire with the electrochemical potential.

Boussaad and Tao proposed an electrochemical etching method [7] for the fabrication of quantum size contacts between metal electrodes. In contrast to the previous methods, the demonstrated method has a self-termination mechanism that can quickly form a desired gap to fit a small molecule and an atom-size, contact with quantized conductance.

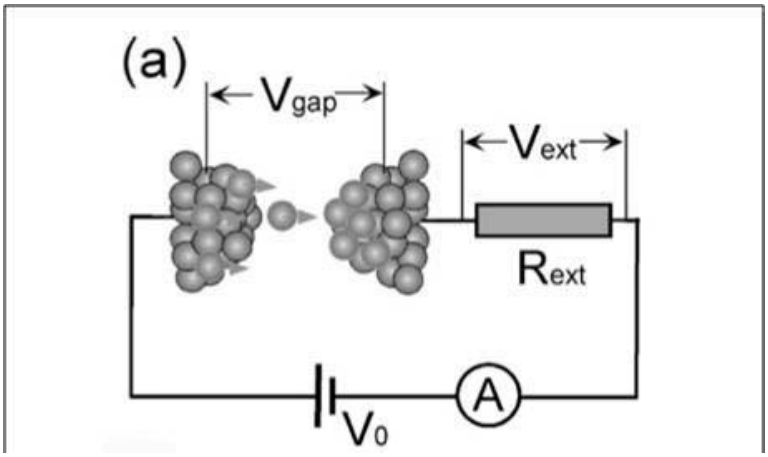

Figure 2.3 – Atoms in gap between electrodes [18]

$$V_{gap} = \frac{R_{gap}}{R_{gap} + R_{ext}} V_0 \qquad (2.1)$$

When applying a bias voltage between two electrodes, metal atoms are etched off the anode and dissolved into the electrolyte as metal ions, which are then deposited onto the cathode. In other words, the dissolved metal ions are guided by the electric field and deposited onto the other side electrode as cathode. R_{gap} is based on conduction through electron tunnelling across the gap and by ionic conduction between the electrodes.

If $\frac{1}{R_{ext}} << \frac{2e^2}{h}$, then a small gap with conductance is formed. In this case, electron tunnelling is replaced by ballistic transport and step wise shape of QPC is more obvious.

If $\frac{1}{R_{ext}} \geq \frac{2e^2}{h}$ then a contact with conductance near a multiple of G_0 is fabricated. Conductance is in logarithmic scale.

The exponential dependence of current on the bias is in sharp contrast to the simple ohmic behaviour of the atomic scale contacts. The current is also several orders of magnitude smaller than that for the atomic scale contacts micro ampere goes to nano ampere. In the second case, the exponential dependence is in good agreement with electron tunnelling across a square barrier.

The self-termination effect is further enhanced by the exponential dependence of the etching and deposition current density, J, on V_{gap}, according to

$$J(V_{gap}) \propto \exp(\alpha e V_{gap} / k_B T) \qquad (2.2)$$

2.2 Discussion of experimental work:

There are several methods to make nanowires that exhibit the conductance quantization phenomenon. Mainly they were based on mechanically breaking a fine metal wire or separating two hetrojunction electrodes in 2DEG or using STM tip pressed on a metallic surface.

A simpler technique has been developed that is based on electrochemical etching and deposition to fabricate metallic nanowires. A self-terminated electrochemical method was used to fabricate atomic – scale contacts between two Au electrodes in a microfluidic channel. The conductance of the contacts varies in a stepwise fashion as a quantum point contact (QPC) with a tendency to quantize near the integer multiples of the conductance quantum (G_0). The principle of this method is sketched in fig. 2.4 below:

$$Au + 4Cl^- \Leftrightarrow Au[Cl_4]^- + 3e$$

When Au is inserted in solution of HCl, there will be a tendency for the metal to pass into solution as ions and also for the ions from the solution to discharge on to the metal. In other words, the two processes represented by the reversible reaction above. All these processes happen just at the surface of electrodes. When equilibrium is attained, and the reversible potential of the electrode is established, the two reactions take place at equal rates. [8]

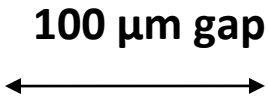

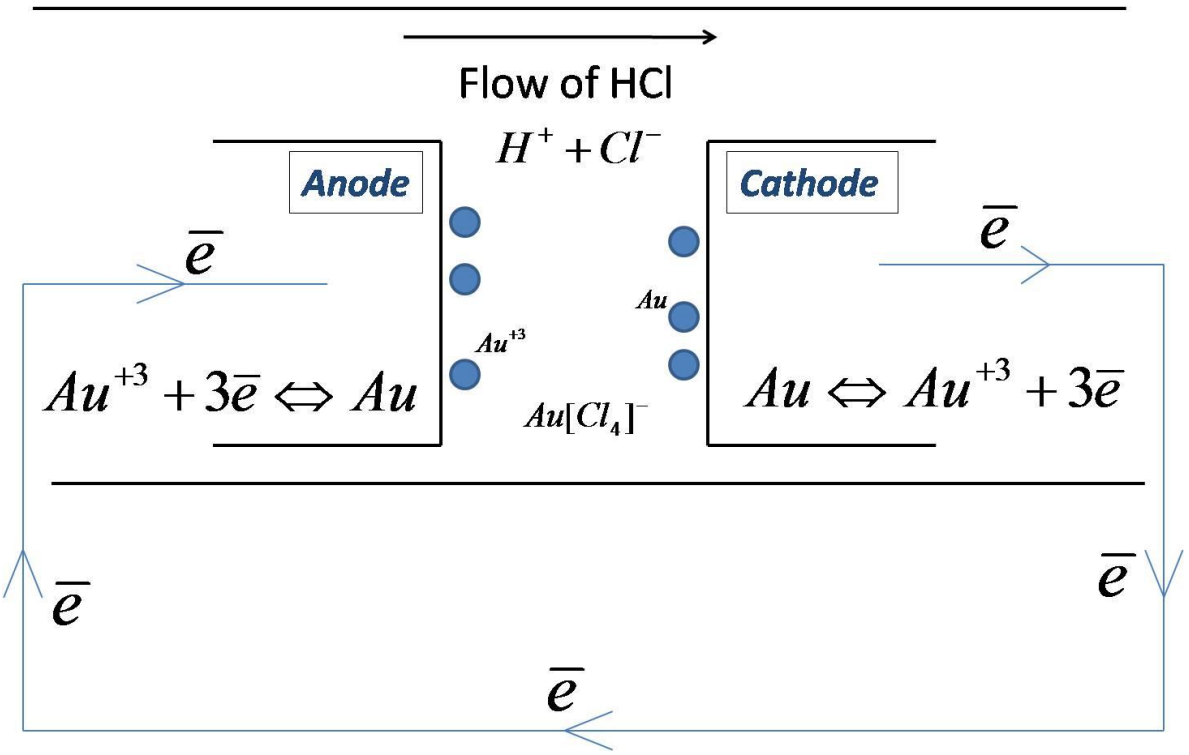

Figure 2.4 - Schematic view of electrodeposition before connecting to potential

The experiment works by a pressure – driven flow parallel to a pair of Au electrodes separated in a relative large gap of 100 μm (for ease of fabrication we choose this gap size) in solution of HCl. Electrodes are showing by label of Anode and Cathode in Fig. 2.4 and microfluidic channel is parallel with them and carrying HCl.

When applying a bias voltage between two electrodes, metal atoms are etched off the anode and dissolved into the electrolyte as metal ions, which are then deposited onto the cathode. Consequently, the gap decreases to the atomic scale and then completely closed as the two electrodes form a contact. In order to fabricate an atomic contact in a controlled fashion, the deposition process must be terminated promptly once a desired gap or contact is formed.

We use electronics to create a self-termination circuit. An explanation for self – termination process can be considered by Fig. 2.5:

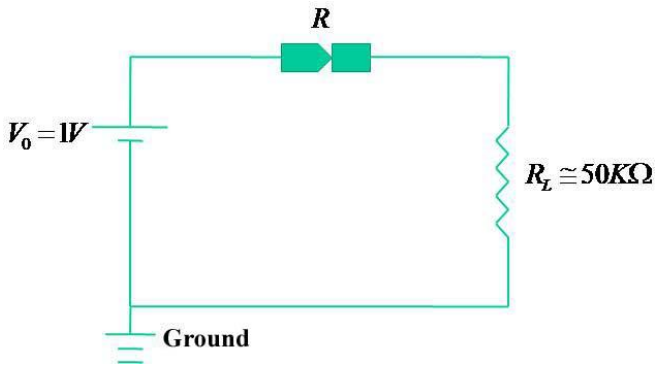

Figure 2.5 – Modeling of experimental setup

If one electrode is connected to an external resistor the effective voltage for etching is given by (same as equation 2.1)

$$V_R = \frac{R}{R + R_L} V_0 \qquad (2.3)$$

where R is the resistance of connection through the gap and R_L is external resistance. V_0 is total applied bias voltage and V_R is voltage across connection which is the effective voltage for deposition. The value for R is based on electron tunnelling across the gap and by ionic conduction between the electrodes.

Diffusion plays one of the main factors here. It is the net transport of material that occurs within a single phase. It happens in the absence of mixing by mechanical means or by convention. The intrinsic nature of particles to perform a perpetual, irregular movement is referred to as Brownian motion, which provides the basic mechanism for diffusion [34].

When experiment starts the initial gap is large and the electron tunnelling is negligible, so $R >> R_L$ and $V_R \sim V_0$, or the entire applied bias voltage is used for etching and deposition. Consequently, the etching and deposition processes take place at the maximum rates. As the gap narrows, the value of V_R decreases, therefore a slowdown in the etching and deposition rates happens. After a while $R \approx R_L$ and $V_R = \frac{V_0}{2}$, the rate slows eventually. When $R << R_L, V_R \sim 0$ which terminates the etching and deposition and results in a gap whose width depends on R_L. If R_L is smaller than $\sim 12.9 k\Omega$ (quantum conductance), a contact between the electrodes is formed which does not have the qualities of a quantum point contact and mostly is like a small connecting wire between gap. It can be said that the tunnelling is replaced with ballistic transport and there is not any more scattering between electrons and atoms so electrons can move freely from one electrode to the other. [7]

The electrochemical rate of Au etching is affected by V_R, thus the current density (J), according to the Butler – Volmer equation:

$$J \propto J_0[\exp(\frac{\alpha_a e V_R}{k_B T})] \qquad (2.4)$$

Where J_0 is exchange current density , α_a and α_c are the anodic and cathodic transfer coefficients respectively, e is the charge of the electron , k_B is Boltzmann's constant , and T is temperature . This exponential dependence on V_R leads to a self – termination effect in the formation of the junction as the electrochemical reaction at the junction effectively halts, because V_R is decreasing. By choosing $1/R_L$ near to the quantum of conductance, G_0, one can select the formation of quantum point contacts [10].

Butler – Volmer equation mentions change of current density. It can be used to calculate by how much the current density changes when the potential difference at an electrode is changed [12]. Generally α shows the sensitivity of the transition state to the applied voltage. If α=0 then the transition state shows no potential dependence. In our experiment we estimated that when *V* changes by 200 mV, *J* decreases by factor of 5 (α=0.5).

2.3 Origin of Self-Termination

We are interested to know the actual electrochemical description of self-termination and how this phenomenon happens in microscopic view. Understanding these concepts will help us to control the processes and parameters in case of getting expected results. The Butler – Volmer equation is supposed to relate current flow and potential difference in an electrolyte solution.

At equilibrium, the flow of charge out of the electrode is equal to the flow towards, but when a bias voltage is applied, there is a net flow of current. However, we are interested in the passage of current in the circuit. Description of this dynamic process depends on setting up a model of the microscopic structure of the interface.

If the electrode has to be made a cathode or an anode in an electrolytic cell, then there is a resultant flow of current. The difference of potential between the electrodes must be made larger so that the rate of the appropriate reaction rate is increased. The relation between the current strength and the potential depends essentially on the nature of the slow stage which determines the rate of electrode process. [8]

If electrons leave the electrode and reduce the cations in the solution, the electrode acquires a positive charge, and by accepting electrons the solution loses its electro- neutrality and

becomes locally negatively charged. The excess negative charge of the solution is confined to the region near the electrode, where there is an attractive interaction with the electrode's net positive charge and solution's negative charge.

The continuous discharge of ions at a cathode involves transfer of ions from the bulk of the electrolyte to the layer of solution in contact with the electrode by diffusion. Also discharge of the ions to form atoms on the electrode and conversion of the atoms to the normal stable form of the deposited substance are important main stages.

2.4 Conclusion and applications

An important example of conductance quantization is in metallic nanowires. It has been proposed that such nanowires may be used as conductors for interconnections in device applications and as single-atom digital switches in nanoelectronics circuits. It also has recently been observed that the conductance quantization is sensitive to the adsorption of molecules onto the nanowires, which may lead to applications in sensitive chemical sensors [24]. For practical applications, however, a suitable method that can mass-produce stable nanowires is needed.

Here we discussed three main methods to fabricate nanowires and consequently quantum point contacts. Also we described a new approach to make quantum point contacts in a more guided way by using microfluidic channel during electrochemical etching gold electrodes.

Fabricating electrodes separated a gap smaller than a few tens of nm, has been a challenge to conventional techniques. Several unconventional methods, including a combination of mechanical controllable break junction, STM tip structures and electrochemical methods have been reported. [22, 23]

Our method involves no mechanical movement; it has, therefore, the potential advantage of being faster, more stable and easier to incorporate the fabricated nanowires into conventional microelectronics than the mechanical methods.

Chapter 3

3. 1 Design and Description of Experiment

Our work was extended by confining the electrochemistry within a microfluidic channel. Others have used different methods which have been explained in previous chapters as related works to this project. But this project has a simpler fabrication method and more mechanical robustness that makes nanowires to resist under strain and be efficient to use in different kinds of connectors.

The channels were patterned in a 2 mm-thick layer of Poly DiMethyl Siloxane (PDMS) and fabricated using soft lithography. The PDMS contained an array of microchannels running parallel to one another that were 2 cm long, 30 μm high and 200 μm wide. Au-coated glass slides (100 nm of Au, 20 nm of Cr, from the Evaporated Metal Films Corporation) were etched to produce gold electrodes with 100 μm gaps between them. The micro channels were aligned over the electrodes, and a Plexiglas cover plate and a clamp provided a mechanical seal between the PDMS and the glass substrate.

The fluid flow was controlled using a Harvard Compact Infusion Pump Model 975 (analogue motor control) and provided flow rates between 0.68 nL/min and 12.4 μL/min using a 10 μL syringe. A solution of 2 M HCl was infused into the micro channels. The Au electrodes were connected in series with a load resistor (~ 50 kΩ) to a current amplifier that monitored when the electrodes had come into electrical contact. Typical values of the applied bias were 0.7 – 1 V.

A CCD camera has been installed on top of experimental chip to record accurate changes in sample and there is a connection between computer and LabView software to control voltage and gathers data of changing current.

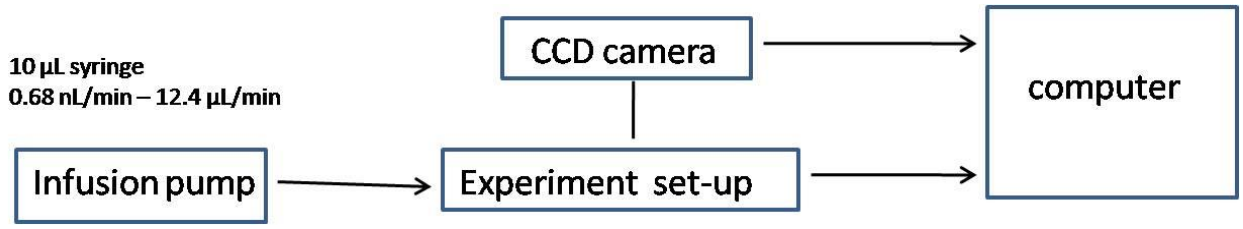

Figure 3.1 – Schematic of the experiment

3.2 Details of making PDMS layer

Because it takes time for warm up, before starting fabrication the hot plate and UV fan should be turned on.

Substrate Pre-treatment: To obtain maximum reliability, the substrate should be clean and dry prior to applying SU-8 resist (a type of polymer).

Spin coating: SU8 resists are designed to produce low defect coatings over a very broad range of film thickness. Starting from one edge and gradually move to other edge with a stick apply SU8-25 on glass slide. Make the layer on glass to thickness of about 25 microns. Then turn on vacuum pump and spin coater and follow recipe #8. It deals with max speed: 2000 rpm/second, ramp: 500 rpm, time 45 s. After spin coating if there are too many bubbles on the surface of glass, put the glass slide away and try other one.

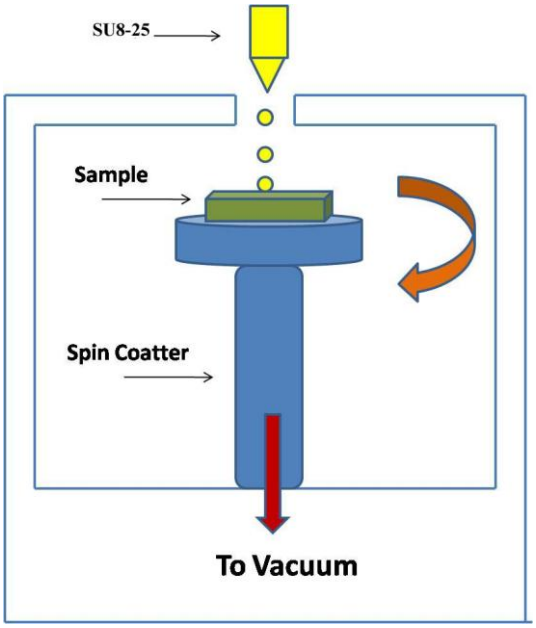

Figure 3.2-Spin coater

Soft bake: After the resist has been applied to the substrate, it must be soft baked to evaporate the solvent and densify the film. Put coated slides on hot plate for time intervals respectively 65˚ C → 3 min, 95˚C → 7 min. After soft bake cool down slides for 2 min in room temperature.

Expose: Put a mask of designed pattern on baked SU8-25 and also put a glass slide on top of them to make it better shaped in photolithography. Put these set in photolithography system under UV lamp (~350W) for exposure time of 45 s. Check power and current of system before turning on UV light. After this put slides on top of hot plate for hard baking.

Post Exposure Bake (PEB): The same as soft bake temperature and timing is respectively: 65˚ C → 1 min, 95˚C → 3 min. Cool them down for 2 min in room temperature

Developing process: Put glass slides in the developing solution and close the lid and turn them gently. Bring out glass slide with tweezers; the patterns on glass slide should be obvious now.

Wash the glass slides with Isopropanol .If there are white spots on glass slide put it back in solution and wash it again.

Rinse and Dry: Following development, the substrate must be washed with distilled water and then air has been blasted gently on it.

Making PDMS: With the ratio of 1 / 10 make PDMS, 30 g (silicon elastomer base), 3g (silicon elastomer curing agent). PDMS should be made in a plastic container first, mix the component with wooden stick and put the plastic container on vacuum oven for degassing (pressure should be 30 in.Hg). Degassing process has been completed when no bubbles coming out to the surface of container. Put 3 slides of baked glass on a container and pour degassed PDMS liquid and put whole set in vacuum again for degassing (about 1.5 hour). Put the container on hot plate for last baking. Temperature would be close by 85˚C and time is 20 min. Let baked PDMS to be cooled down. Cutting PDMS in pieces that desired to use for experiment can be done now. Make holes in PDMS by using a press. It is better to align holes with a mask before or use a pen for mark holes on PDMS. If you leave PDMS after degassing for 24 hours in room temperature, it will be cured without using last bake on hot plate (but binding of inside structure may be different with what is expected). Naturally PDMS is hydrophobic (doesn't like water) so if it is needed to absorb water, we can make it more hydrophilic (to like water) by doing plasma treating on the surface, but it is temporary and after 3-4 days it comes back to its natural state. Also if there are bubbles inside PDMS they go out of it. Also PDMS doesn't keep gas inside.

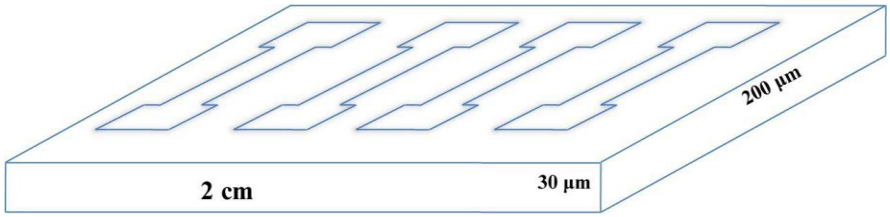

Figure 3.3- Side view of PDMS

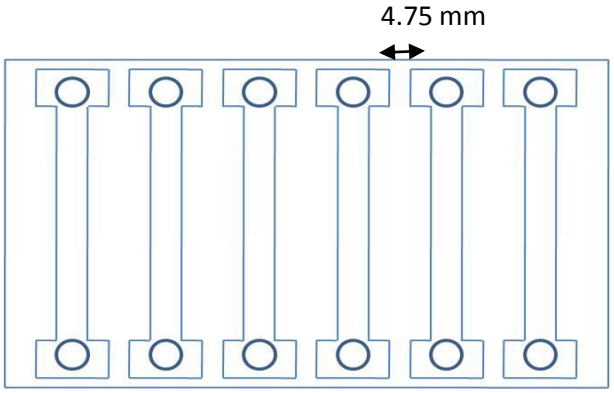

Figure 3.4 – Top view of PDMS

3.3 Details of making gold slides

Making gold slides are the same as making PDMS with the difference that the process finishes in the developing process after drying by air. A chemical solution is used for cleaning gold slides and getting fresh gold slides without any pattern remained from developing level. But it is hazardous materials refer to safety instructions in hand books.

Etching gold slides: put gold slide in gold – etching solution for about one minute. Bring it out and wash it with distilled water and isopropanol. If any gold remains at edges or gap between

channels do above process again. Put the etched gold slide in Chromium-etch liquid for 30 – 40 sec .Wash the slide with distilled water. It there is gold on the slide don't put it in Chromium liquid because this makes it too hard for etching and removing gold. Put gold slide after Chromium etch in acetone to remove SU8 (This would takes about 5 – 15 min). If still there is SU8 on gold slide, put it in ultrasonic system and let it remove SU8 gently (about 0.5 – 1 hour). Bring etched gold slide out of ultrasound and let it to be dried at room temperature.

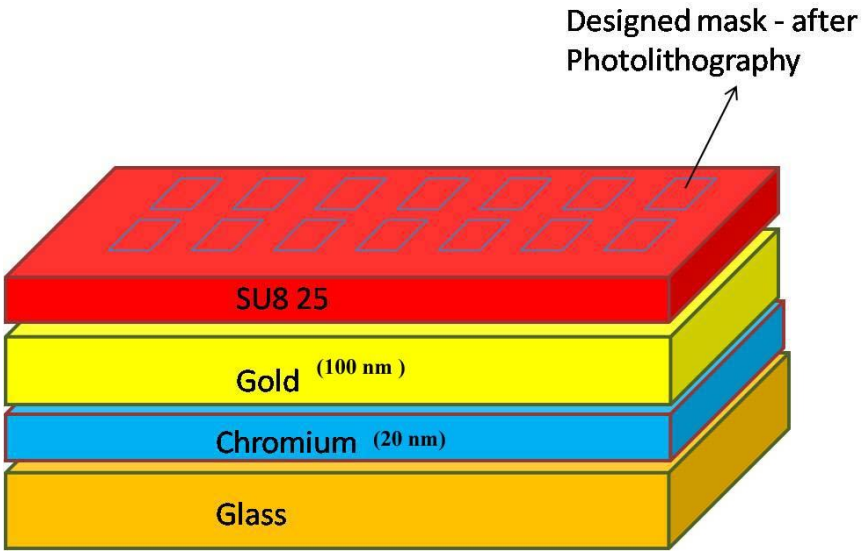

Figure 3.5 – Side view of gold slide

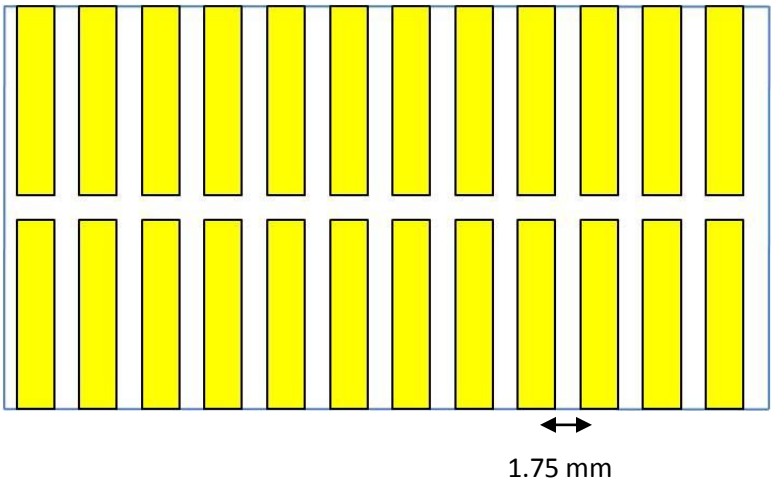

Figure 3.6 – Top view of gold slide

3.4 Details of plasma treating

Plasma treating has been used for better binding between gold slide and PDMS. Because of energy expansion plot (shown in fig. 3.7 - 3.9) inside plasma treating system, it is more efficient to follow this way to put samples in it.

Positioning sample: Before starting plasma treating washing PDMS and gold slide with isopropanol helps better matching situation. First put glass slide on top part of cylindrical wires in the mid part of system. Then put PDMS sample on another glass slide on the bottom of cylindrical wires but in the mid part of system.

Plasma treating: Turn on vacuum pump for 2 – 3 min to make vacuum inside the chamber. Turn on system and change RF level to MED and slightly loose the vacuum screw and let a bit air gets inside to make plasma. After appropriate time (usually 45 s) when chamber changed color from purple to pink turn off RF switch. Turn off vacuum pump and let air get in and put out PDMS sample and glass slide. Now put PDMS and gold slide on top of each other in expected position

on designed mask. It is important to know which part should be faced up inside plasma treating system because effect of plasma is dangling bonds of sides which should touch each other and bind to each other. (The center of chamber in the plasma treating system has much moe energy than the edges. This has been shown in fig. 3.8)

Baking for binding: Put whole set on top of hot plate for 5 min under 85˚C to make binding.

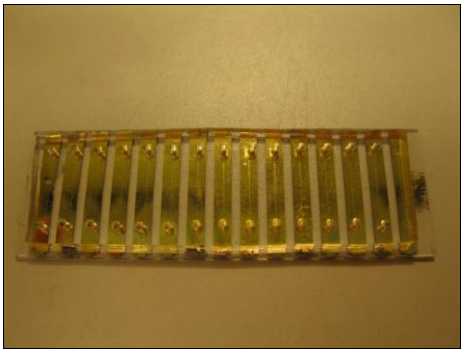

Figure 3.7 – Picture of PDMS and gold slide

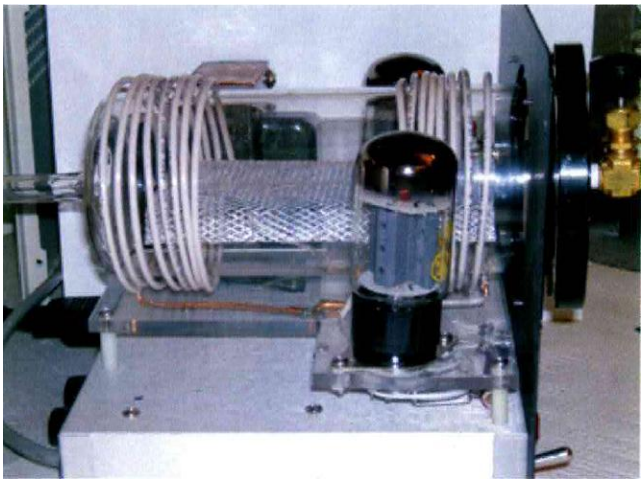

Figure 3.8 – Plasma treating system

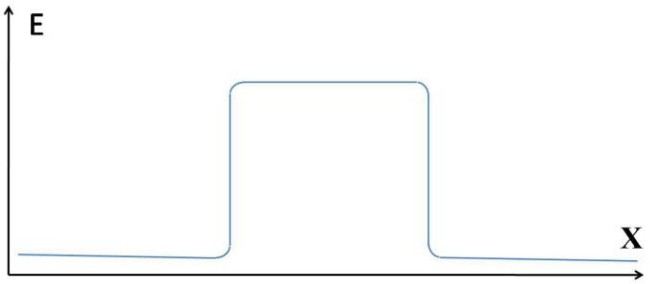

Figure 3.9 – Level of energy inside the plasma treating system

Figure 3.10 – Working plasma treating system

The whole process of fabrication can be shown in an algorithm with proceedings as below:

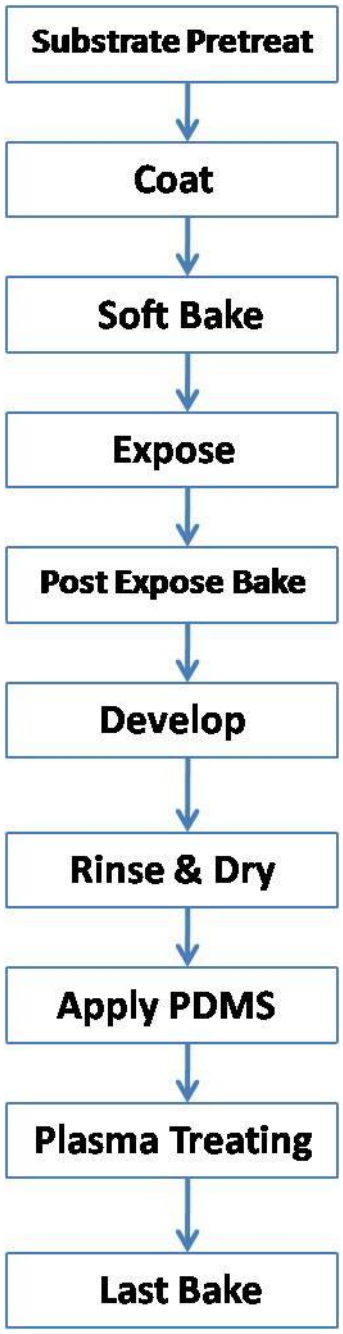

Figure 3.11 – Steps of fabrication

As it mentioned before for making PDMS samples complete process must be done up to applying PDMS and for making gold slides fabrication should be stopped in rinse and dry level. And for binding two slides of PDMS and gold the last two levels must be done.

3.5 Clamping the set up

When gold slides and PDMS have been made and plasma treating has been applied on them, the actual chip is ready to go. Then we thought about a system for clamping. Because it has been needed to have actual set up for pumping HCl inside chip and doing electrochemical process. As mentioned before in the beginning of this chapter we used a Plexiglass plate in the top and bottom of chip and made holes on it for letting HCl go through tiny tubes.

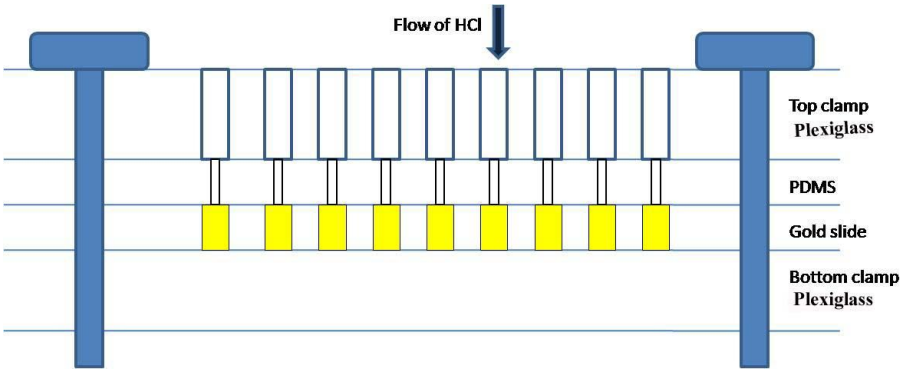

Figure 3.12 – Side view of clamping

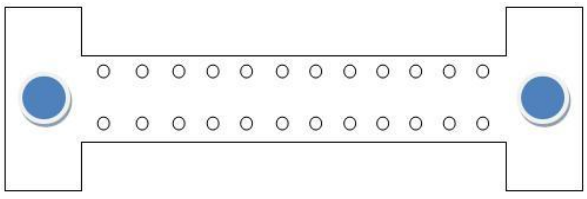

Figure 3.13 – Top view of clamping

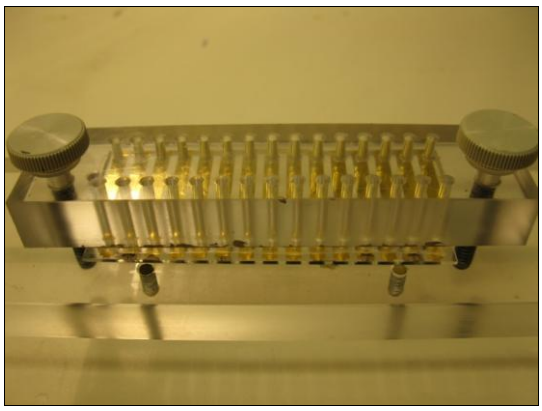

Figure 3.14 – Picture of clamped set up

We pumped HCl with different speeds inside this set up and analyzed effect of changing this parameter to shape of growth of Au. After finishing experiment we used an empty syringe and with a connected tube to the hole in other side of channel make suction to take out liquid and wash channel afterwards.

I will talk about implementation and results that we got from this experimental set up and compare them together at different regimes in a separated chapter.

3.6 Electrical set-up of Experiment

An electrical circuit has been designed to find dependence of resistance in connected gap (R) with outer voltage (V). There is an op-amp which amplifies small signal in circuit and has a big gain.

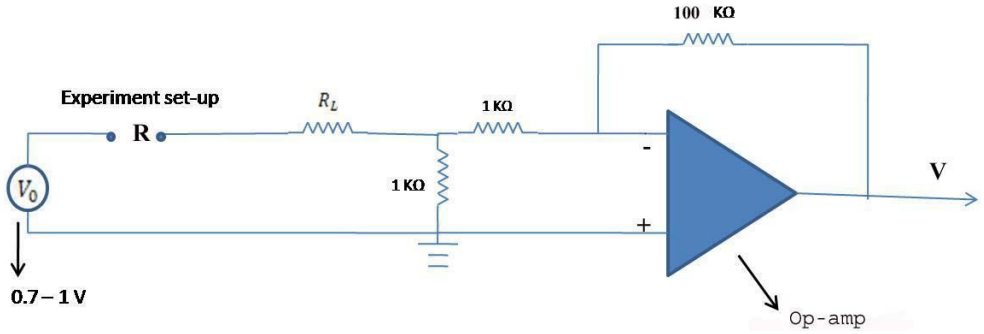

Figure 3.15 – Schematic of the electrical circuit

For analyzing Op-amp circuit two fundamental rules should be obeyed:

1) Input impedance of negative and positive heads is infinity

2) With feedback, op-amp will try to make $V_+ = V_-$

For simplicity I changed the name of resistances in this circuit to more general ones as below:

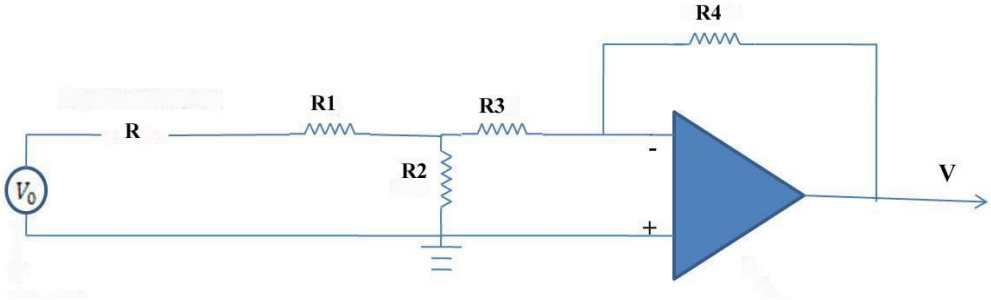

Figure 3.16 – Electrical circuit with actual resistances

Extracted equation for $R(V)$ would be:

(Assuming $R_2 = R_3$)

$$R = \frac{-1}{2}\frac{V_0}{V}R_4 - R_1 - \frac{R_2}{2} \qquad (3.1)$$

And error is as below:

$$\Delta R = \frac{1}{2}\frac{V_0}{V}\Delta R_4 + \frac{1}{2}R_4\frac{\Delta V_0}{V} + \frac{1}{2}R_4\frac{V_0}{V^2}\Delta V + \Delta R_1 + \frac{1}{2}\Delta R_2 \qquad (3.2)$$

Values for some quantities are:

$Gain \cong -100,\ Offset: -0.003\text{V},\ R_L = 51.57\ \ K\Omega,\ \ R_2 = 1\ \ K\Omega,\ R_4 = 100\ \ K\Omega$

$\Delta R_1 = 0.1,\quad \Delta R_2 = 0.01,\quad \Delta R_4 = 0.1,\ \ \Delta V_0 = \sqrt{V_0}$

And equations can be as these ones:

$$R = -(500 + 51.57K + 50K\frac{V_0}{V - offset}) \qquad (3.3)$$

$$V = \frac{50K \times V_0}{-(R + 500 + 51.57K)} + offset \qquad (3.4)$$

As we know from electrostatic relations, conductance is inverse of resistance.

$$R = \frac{1}{G} \qquad (3.5)$$

And conductance can be quantized by equation below:

$$G = n(\frac{2e^2}{h}) \quad n = 0,1,2,3,... \qquad e = 1.6\times10^{-19}C\ \ ,\ \ h = 6.62\times10^{-34}\ \ m^2kg/s \qquad (3.6)$$

$$R = \frac{1}{n}\frac{h}{2e^2} \qquad , \qquad \frac{h}{2e^2} = 12949.2188 \qquad , \qquad R \approx \frac{1}{n}\times 12949.2188 \qquad (3.7)$$

A quantized equation for relating output voltage and resistance is:

$$V = \frac{50K \times V_0}{-(\frac{1}{n}\frac{h}{2e^2} + 500 + 51.57K)} + offset \qquad (3.8)$$

And at the end a relation for quantization steps related to output voltage is:

$$n = \frac{-12949.2188}{50K + \frac{V_0}{V - offset} + (500 + 51.57)} \qquad (3.9)$$

Gain of electrical circuit: $\frac{\Delta V_{out}}{\Delta V_{bias}} = \frac{0.9368 - (-0.9382)}{(-1.0007) - 0.9986} = -0.9378$ (3.10)

Slope is V-out / V-bias which is gain of op-amp and intercept is off-set of output voltage in our data.

3.7 Troubleshooting of the experimental data

After data analysing and plotting, it has been found out that there was a difference in calculated values for resistance through mentioned formula in previous part and the measured values for resistance between gap in actual set up. Examples of this difference are mentioned in table below.

Sample Name	Calculated Resistance	Measured Resistance
AAI-05	3.8 – 6.2 kΩ	0.8 Ω – 4 Ω
AAD-01	4.3 – 6.6 kΩ	2.8 – 6.3 Ω
AAH-13	3.2 – 6.6 kΩ	12 – 13 Ω

Table 3.1 – Difference of data

For troubleshooting of this problem we decided to make a calibration table of the different values of V_{out} and finding their correspondent value for Resistance by using a variable resistance box. Table below is a sample of calibrated values of actual set up:

R(Ω)	V_{out} **(Volt)**	**R(Ω)**	V_{out} **(Volt)**	**R(Ω)**	V_{out} **(Volt)**	**R(Ω)**	V_{out} **(Volt)**
0	0.943	1000	0.926	8000	0.820	60000	0.444
10	0.943	2000	0.909	9000	0.807	100000	0.329
60	0.942	3000	0.893	10000	0.794	200000	0.200
100	0.941	4000	0.878	20000	0.686	300000	0.144
200	0.939	5000	0.862	30000	0.604	400000	0.113
500	0.935	6000	0.848	40000	0.539	500000	0.093
900	0.928	7000	0.834	50000	0.487	600000	0.080

Table 3.2 – Calibrated data

The next work was comparing values of these calibration data with output of the electrical circuit simulated with PSPICE (simulated circuit was the same as our experimental circuit). This comparison proved that calibrated data were according to actual set up and they are very accurate.

Calibration Data		Simulator Data		
R	**Vout**	**Vb**	**Vout**	**Difference**
0	0.943	-0.009524	0.932390	0.011251
10	0.943	-0.009522	0.932140	0.011516
60	0.942	-0.009513	0.931300	0.011359
100	0.941	-0.009506	0.930641	0.011009
200	0.939	-0.009488	0.928898	0.010758
500	0.935	-0.009435	0.923710	0.012075
900	0.928	-0.009365	0.916882	0.011981
1000	0.926	-0.009347	0.915191	0.011673
2000	0.909	-0.009117	0.898616	0.011424
3000	0.893	-0.009013	0.882633	0.011609
4000	0.878	-0.008855	0.867209	0.01229
5000	0.862	-0.008702	0.852317	0.011233
6000	0.848	-0.008554	0.837928	0.011877
7000	0.834	-0.008412	0.824019	0.011968
8000	0.82	-0.008274	0.810565	0.011506
9000	0.807	-0.008140	0.797544	0.011717
10000	0.794	0.008011	0.784936	0.011416
20000	0.686	0.006912	0.677833	0.011905
30000	0.604	-0.006077	0.596511	0.012399
40000	0.539	-0.005422	0.532661	0.011761
50000	0.487	-0.004894	0.481199	0.011912
60000	0.444	-0.004460	0.438839	0.011624
100000	0.329	-0.003289	0.324738	0.012954
200000	0.2	-0.001981	0.197279	0.013605
300000	0.144	-0.001414	0.142017	0.013771
400000	0.113	-0.001097	0.111148	0.016389
500000	0.093	-0.000895	0.091442	0.016753
600000	0.08	-0.000754	0.077770	0.027875
700000	0.069	-0.000652	0.067730	0.018406
800000	0.062	-0.000573	0.060043	0.031565

Table 3.3 – Comparing calibration and simulation data

Then we compared the values of resistance calculated by formula from experimental set up with calibrated data. This showed an obvious difference in very high voltages where the values of resistance are very small. (table below)

By tracking current and voltage in different components of simulated circuit and comparing with our calculated values with mentioned formula, we got good evidences that Op-amp was not working linear as expected. So its behaviour cannot be part of our calculations.

Experiment Vout (Exp.)	Vb	Vo	Simulated R	Calculated R	Difference
0.00275	-2.8E-05	-0.99762	18086475	1.81089 E7	-22424.5
0.02075	-0.00021	-0.99792	2352557	2.35232 E6	236.506
0.02777	-0.00028	-0.99762	1744149	1.74408 E6	68.9413
0.03235	-0.00032	-0.99792	1490310	1.49036 E6	-49.7836
0.03906	-0.00039	-0.99792	1225349	1.22528 E6	69.35484
0.04333	-0.00043	-0.99792	1099465	1.09933 E6	134.7334
0.0473	-0.00047	-0.99762	1002497	1.00245 E6	46.59619
0.05157	-0.00052	-0.99791	915459.6	9.14493 E5	966.5715
0.05676	-0.00057	-0.99762	826735.5	8.26689 E5	46.49683
0.05981	-0.0006	-0.99731	781661.8	7.94820 E5	-13158.2
0.06012	-0.0006	-0.99792	777870.1	7.77870 E5	0.11976
0.07752	-0.00078	-0.99762	591389.8	5.91431 E5	-41.2477
0.09216	-0.00092	-0.99792	489336.3	4.89318 E5	18.25
0.10223	-0.00102	-0.99823	436157.5	4.36157 E5	0.526166
0.23962	-0.0024	-0.99792	156159.7	1.56473 E5	-313.303
0.32379	-0.00324	-0.99823	102077.8	1.02077 E5	0.750085
0.8844	-0.00884	-0.99762	4330.95	4.33094 E3	0.009796
0.88623	-0.00886	-0.99762	4214.486	4.21448 E3	0.005969
0.89355	-0.00894	-0.99792	3770.188	3.77018 E3	0.008014

Table 3.4 – Comparing experimental and simulated data

We decided to fit the calibrated data to a graph and consider that the fit-function would be good substitute to the calculated formula. We used the interpolation method to fit the data. The result has been showed in a graph below, where y is V_{out} and x is Resistance.

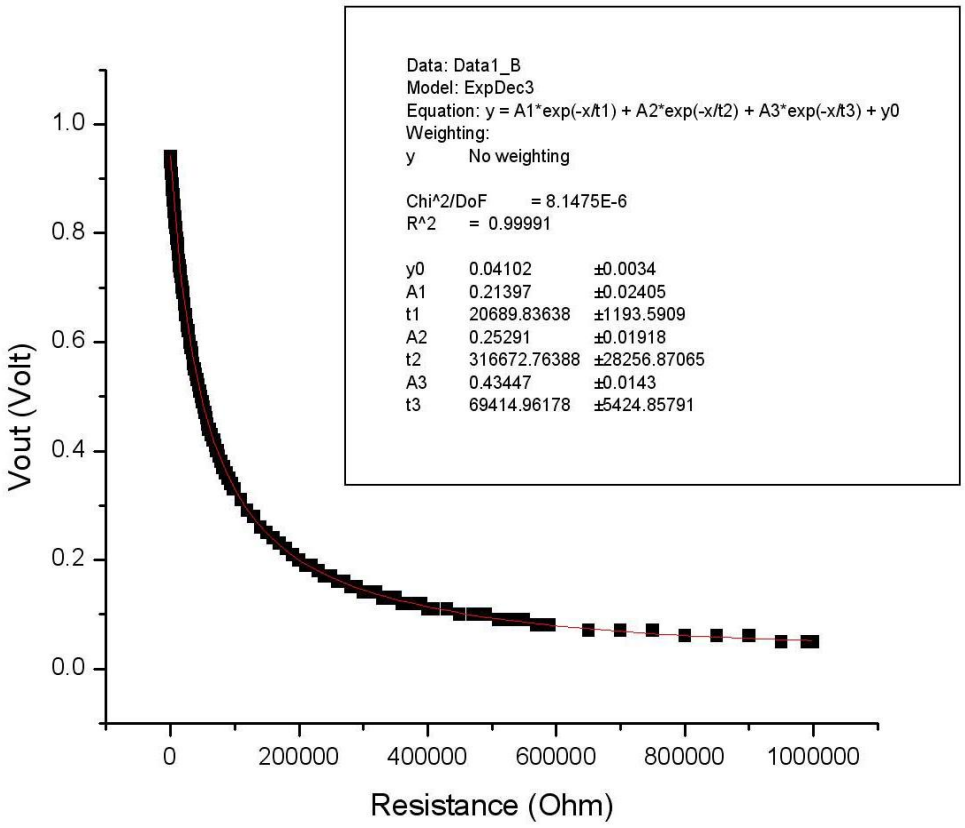

Figure 3.17 – Nonlinear fit of calibration data

Finding the equation for relation with Resistance and output voltage was not very relevant, so we decided to leave this fit function and find out another way of sorting experimental output voltage with calibrated Vout-Resistance data. And using calibration table and sorting data manually was the ultimate process.

Because there was huge number of data points in each sample's experimental raw data, sampling has been done for regions of changes according to Vout-time graphs. Most sampling has been done in places that connection happened and there were jumps in the voltage from minimum to maximum values. For sorting sampled data this algorithm was defined: in calibrated

measurement intervals between average values of two successive output voltage data points can be considered as boxes. Height of this box is related resistance to first output data point. Each sampled data point from experimental output voltage that can be put in these boxes will have the correspondent resistance as the height of the box. By using this method sampled data can be sorted with their related resistance values.

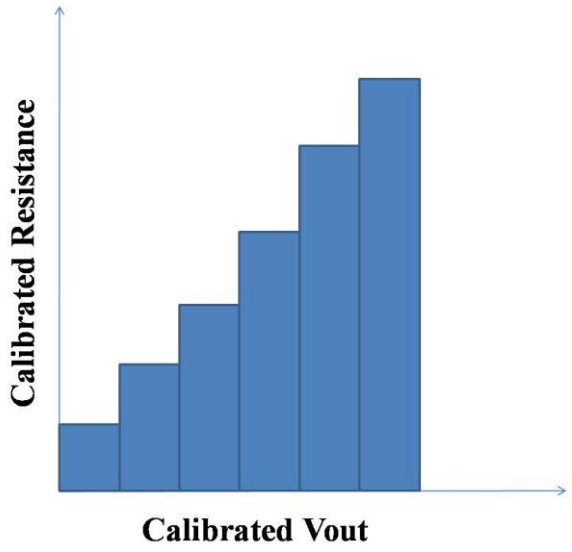

Figure 3.18 – Sorting method of experimental data with calibration data

The results showed better and more accurate values for resistance in compare to previous method. And number of conductance became higher. But still there are some differences. They can be reasoned from limitation of electrical circuit which originally did not designed for very accurate measurements of voltage changes. Also there were noises which make obvious oscillations in higher voltages.

Graph below is result of data analysis. It will be discussed in detail in results chapter.

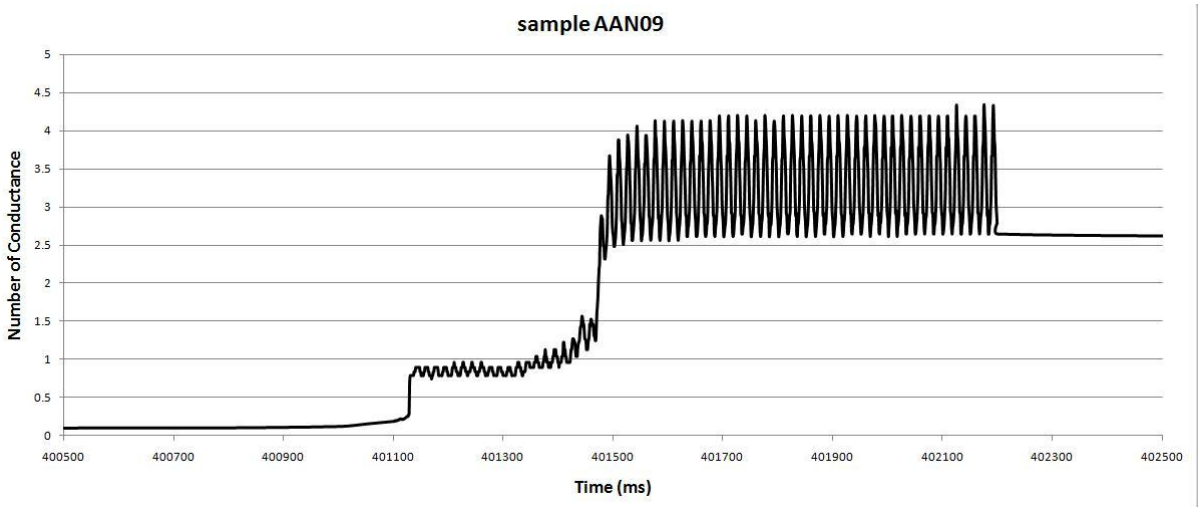

Figure 3.19 – Sample AAN09 - plot of Number of conductance vs. Time

Chapter 4

As explained in chapter 2, the proposed technique in this research has been based on some part of the work of Boussaad and Tao [18]. They got an electrochemical approach in growth of gold ions between macroscopic electrodes that can culminate in a nano-scale junction. Understanding and controlling this process will enable the precise positioning of reproducible geometries into nano-electronic devices.

Details of theoretical base and experimental setup of our work have been mentioned in chapter 2 and 3 respectively. It was extended by confining the electrochemistry within a microfluidic channel. A pressure driven flow is applied during the deposition process in the anode to cathode direction in an effort to influence ion transport. As an additional control parameter, applied flow has the advantage that it is independent of the electrode chemistry and applied voltage to which electromigration and electrochemistry are coupled.

4.1 Contents

In this chapter, at the beginning, important parameters and calibrations that must be considered before starting the experiment will be reviewed and discussed. Then some optical images and SEM photos of result come to show growth-coverage in the gap between electrodes. This is followed by comparing growth-coverage with actual gap size of each sample. Estimated weighted error percentage for coverage of samples at different speeds can be figured out in the graph trend. This graph is relating expected theory and experimental results of desired Quantum Point Contacts together. Afterward there are plots of V_{out} vs. time and number of conductance vs.

time. The first one declares when and where connection happens and the second one will be the answer of questions of “Is conductance quantized” or “Is it showing a step-wise trend?”. Then some electrochemical explanations will come about subjects that happen in output voltage which includes time-scale and amplitude parameters.

As a conclusion we will compare our results with Boussaad and Tao’s work and try to reason about effectiveness of microfluidic channels and illustrating the possibility that we got real QPC. Source of errors were noises and several difficulties to set microfluidics that will be discuss in detail. Future work and suggestions for later improvements on this research is the last part.

4.2 Conditions of experiment

For all samples, it has been tried to keep these parameters constant:

1) Bias voltage: 1 Volt

2) Concentration of HCl as electrolyte: 2 M

3) Designed gap size between electrodes: 100 μm

And the only variable parameter was speed of flow in the microfluidic channel. This makes talking about changes of growth shape vs. speed possible.

Before turning on electrical circuit we did a calibration with output voltage and bias voltage which the graph was showing the gain of electrical circuit for further calculation of conductance.

4.3 Different growth coverages in the gap

There are some discussions about shape of growth at different flow rates and comparing their amount of coverage in the gap size. Five different rate of flow are concerned in this part. They are: without flow, very slow flow (rate 30), slow flow (rate 28), fast flow (rate 22) and very fast flow (rate 16). (These rate are some calibrated numbers in the infusion pump, the actual speed of flow has been calculated and are available in details of each image of results.)

Details of images that have been taken from SEM, optical and video data, mentioned under each image. These data contains estimated gap size from fabrication, speed of flow, coverage and error.

4.3.1. Without flow regime

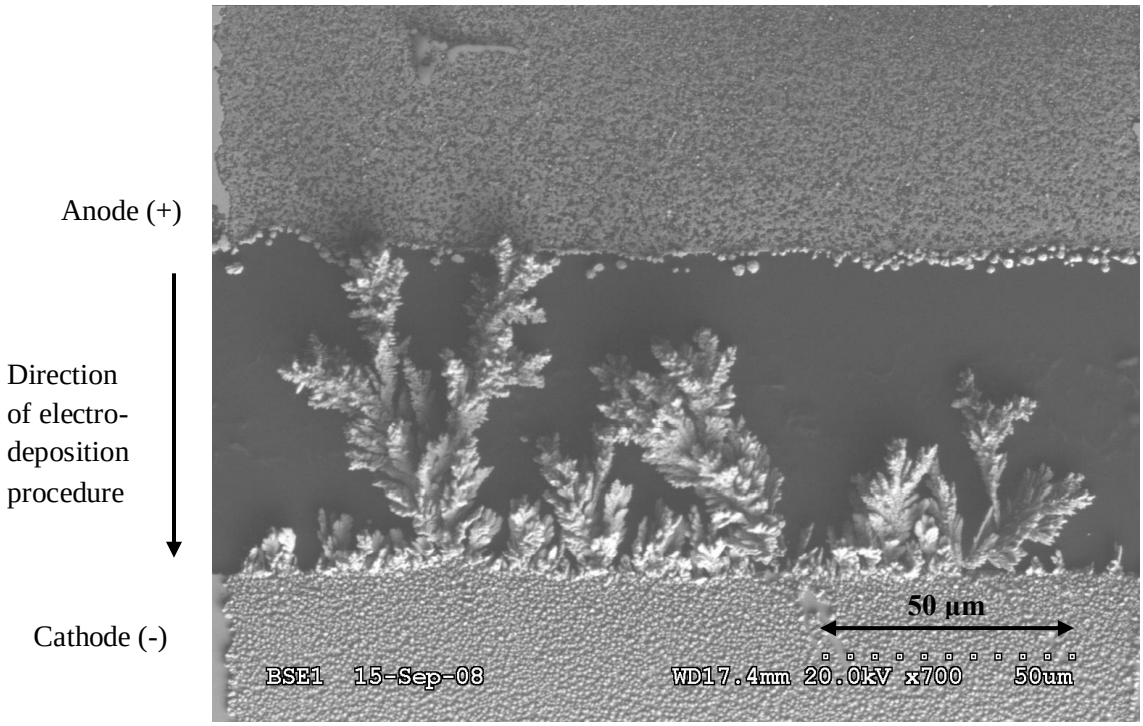

Figure 4.1 – SEM image of without flow regime of AAD-03 sample

Fabricated gap size estimation	Speed of flow	Coverage
$185(\mu m) \times 66(\mu m)$	Zero	0.333 ± 0.006

Dendrite growth is obvious in Fig. 4.1. Ions move from one electrode to the other side deciding where to sit and deposition is forming in a regular way. Fractal shape patterns were growing in about 40 minutes and because finger-shape parts are so sensitive, processes for cleaning up channel with water after deposition should be done very carefully. Any movement must be avoided in case of not damaging the sample.

4.3.2. Very slow flow regime

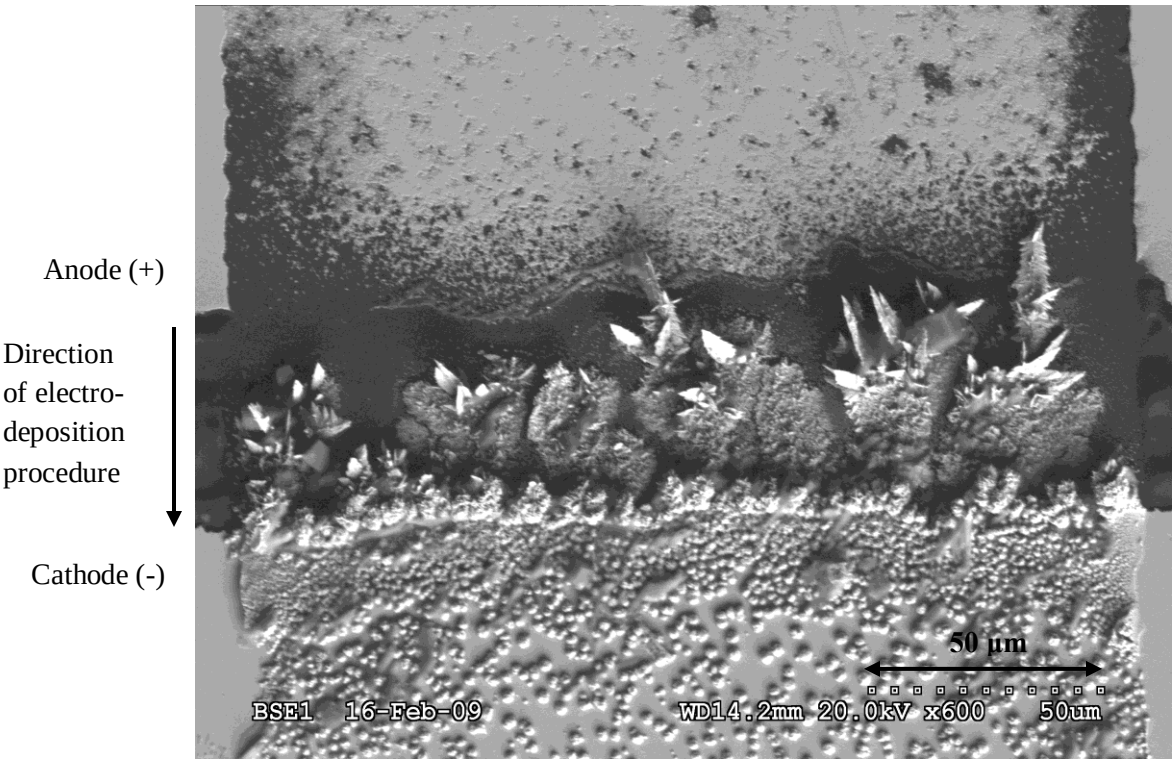

Figure 4.2 – SEM image of very slow speed of Feb-Ch11 sample

Fabricated gap size estimation	Rate of flow (30)	Speed of flow	Coverage
$353(\mu m) \times 87(\mu m)$	0.7 µL/min	0.516 mm/s	0.511 ± 0.004

Difference between Fig. 4.2 and Fig. 4.1 is showing that by using a flow of HCl between electrodes, ions have less time to decide where to sit and the growth is less in regular order shape. But still some fractal end shapes are obvious at connecting points. Fabrication procedure cannot be exactly the same for each set of samples, so some spots is showing in the bottom electrode. These are defects of experimental fabrication of developing level.

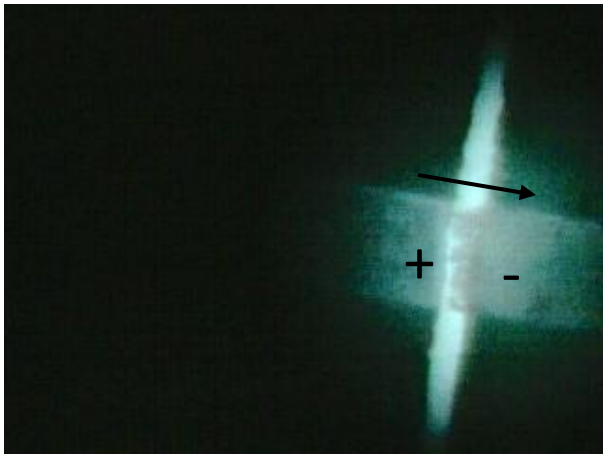

Figure 4.3 – Video image of very slow regime of Feb-Ch11 sample

Video image is showing the same channel's condition as an image shot of video capturing during running the experiment. We set a CCD camera on top of experimental setup so changes in coverage of gap can be recorded as well. It is captured by using graphical software. This frame is showing the moment that connection happed. Left electrode is etched and metal ions sit on the right side.

4.3.3. Slow flow regime

At flow rate of 28 still some regular growth shaping are obvious. Fractal structures also are at tip of connections. At the left edge of channel a connecting finger continues to the surface of top electrode and did not stop at the cathode line. Because of some ions internal movement in the solution, even after self-termination disconnection of circuit, they can accumulate to connecting finger. So in some of the samples growth is stopped but ions still moving to find a place and after a while a steady state will happen in the gap.

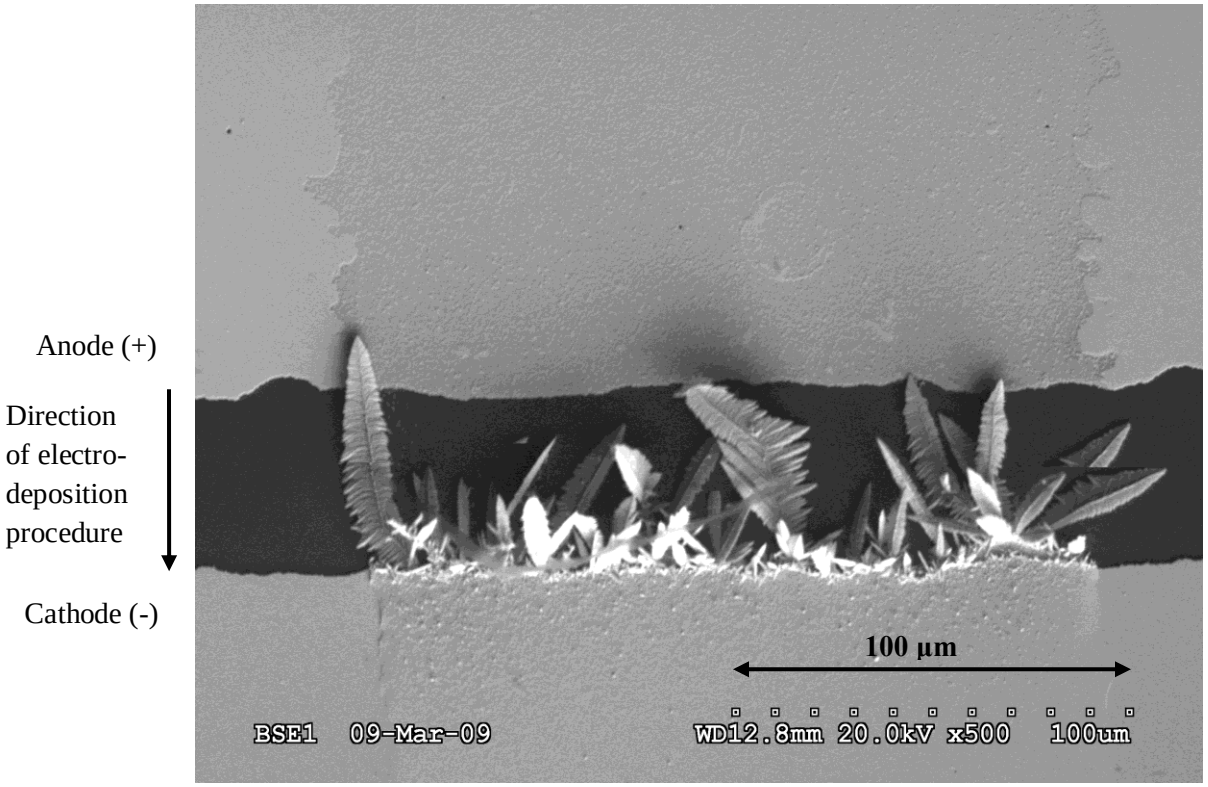

Figure 4.4 - SEM image of slow speed of AAI-Ch03 sample

Fabricated gap size estimation	Rate of flow (28)	Speed of flow	Coverage
$276(\mu m) \times 70(\mu m)$	1.4 µL/min	1.197 mm/s	0.432 ± 0.004

4.3.4. Fast flow regime

At fast rate, more ions is filling the gap space. So coverage increases in compare to previous cases. And the shape of growth is more robust than dendrite shape and there are less fractal shapes appearance.

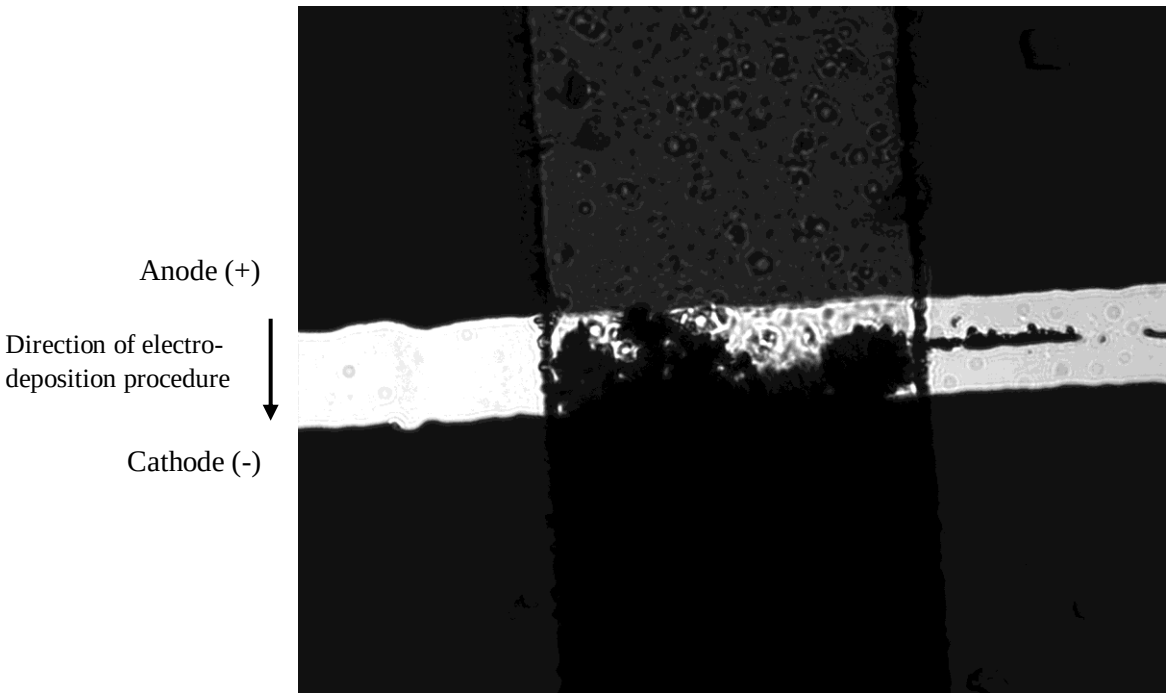

Figure 4.5 - Optical image of fast speed of AAN-Ch09 sample

Fabricated gap size estimation	Rate of flow (22)	Speed of flow	Coverage
$318(\mu m) \times 102(\mu m)$	10.4 µL/min	5.364 mm/s	0.590 ± 0.009

4.3.5. Very fast flow regime

Very fast rate is about 100 times faster than very slow rate. It takes about 15 minute for the growth to accomplish. And much more volume of gap is filled with ions. They sit on top of each other and thickness of growth is higher. This helps to get more concrete and stronger structures

that can be used in systems with mechanical micro strains. Two SEM images below are showing quality of this type of growth.

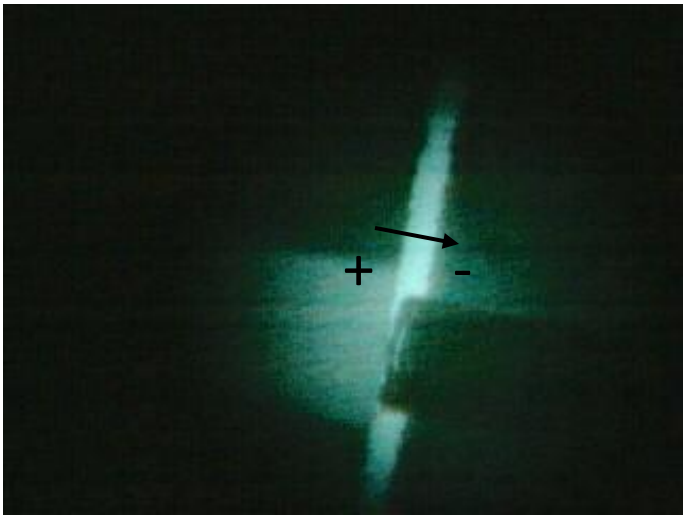

Figure 4.6 - Video image of very fast regime of Feb-Ch09 sample

Fabricated gap size estimation	Rate of flow (16)	Speed of flow	Coverage
$220(\mu m)\times 84(\mu m)$	78.5 µL/min	70.752 mm/s	0.612 ± 0.106

Figure 4.7 - Video image of very fast regime of Feb-Ch14 sample

Fabricated gap size estimation	**Rate of flow (16)**	**Speed of flow**	**Coverage**
$244(\mu m)\times 84(\mu m)$	78.5 μL/min	63.794 mm/s	0.573 ± 0.089

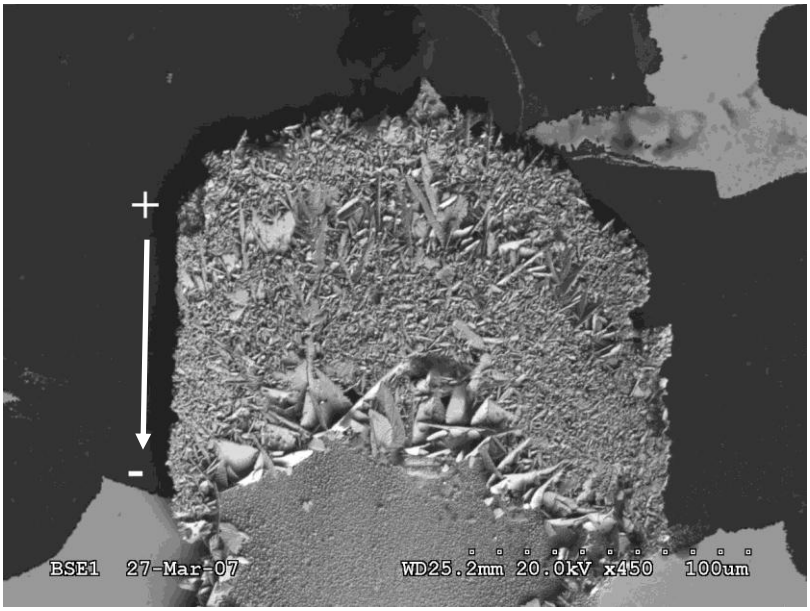

Figure 4.8 – Top view of SEM image of very fast speed of DZ-Ch10 sample

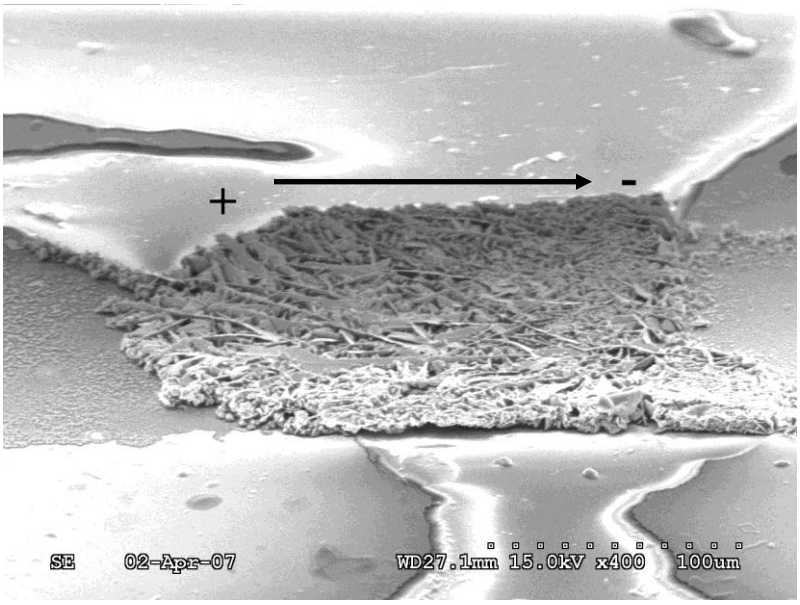

Figure 4.9 – Side view of SEM image of very fast speed of DZ-Ch10 sample

Preciseness of data gained from SEM, optical and video images are different from each other in case of contrast, magnification and resolution. Estimated factor for converting these

parameters to have a smooth and comparable data is the ratio of SEM to optical is 1/4 and SEM to video is about 1/16. So because of these approximations trend of coverage and error has ups and downs. The numbers mentioned here are just some samples to show qualifications of different shapes. We made many samples and what we get as a result is averaging over several samples to predict general behaviour of system.

Name	Rate	Speed (mm/s)	Gap size	Coverage	Error	Comment
AAD-03	0	0	$185(\mu m) \times 66(\mu m)$	0.333	0.005	SEM
Feb-Ch11	30	0.516	$353(\mu m) \times 87(\mu m)$	0.511	0.004	SEM
AAI-ch03	28	1.197	$276(\mu m) \times 70(\mu m)$	0.432	0.004	SEM
AAN-ch9	22	5.364	$318(\mu m) \times 102(\mu m)$	0.590	0.009	Optical
Feb-ch09	16	70.752	$220(\mu m) \times 84(\mu m)$	0.612	0.106	Video
Feb-ch14	16	63.794	$244(\mu m) \times 84(\mu m)$	0.573	0.089	Video

Table 4.1 – Result of comparing different coverages

4.4 Discussion of different flow rates' shape and coverage

Following all images will give a good view of how growth shape changes by increasing speed of flow in the microfluidics channel. At without flow regime a branched growth of dendrite structure was observed. This means by keeping a drop of HCl in the gap between Au electrodes, ions tried to find their way along the gap and gradually electrodeposition movement takes place. In this process ions have enough time to decide about their direction and where they want to sit. So kind of ordered crystallization happens in the gap. This procedure is called diffusion limited aggregation.

When we come along the trend of increased speed of flow, an important improvement is the higher amount of coverage. That is a sign of filling more space in the gap with ions of Au and become more robust. Dendrite morphologies exchange by densely packed robust colony of ions which become narrower and cone-like shape at the cathode. These structures don't have any branches or finger shape growth and ions cannot decide quickly as HCl flows in the channel. So they just come in to the gap and find an available place and sit. This procedure is called ballistic deposition.

The shape of contact is also different. At slow speeds the connection looks more sharp and narrower so it has more probability to form a quantum point contact. By increasing the speed of flow the connection's cross section becomes bigger and less considerable as tiny structures like nano wire or QPCs.

Bias voltage from cathode to anode works as a guide for ions to show them the direction of movement and push them to move from electrode to electrolyte and then to the other electrode. This helps electrodeposition to happen and connection will form afterward. The role of microfluidics channel is to improve guiding ions in the deposition process. But sometimes

because of screening effects potential cannot work as a good guide. By help of the flow of electrolyte (HCl), ions of electrode move faster and in more numbers. So the effect of higher speed is obvious in fast flow regimes.

We run the experiment for several times with different flow rates. Images mentioned above are some samples at different speeds. Through using weighed average at different speeds, we tried to find a connection between expected theories of observed experiments. Result was an exponential graph that is increasing form slow speed of flow to fast ones.

It should be mentioned that at explained five different rates, rate and order of speed also changes exponentially from zero flow speed to very fast speed. So increasing from rate 30 to rate 16, change of speed is really fast.

In our recently submitted paper we talked about whole process and emphasis on relating aspect trend of growth change in theory and experiment. [22]

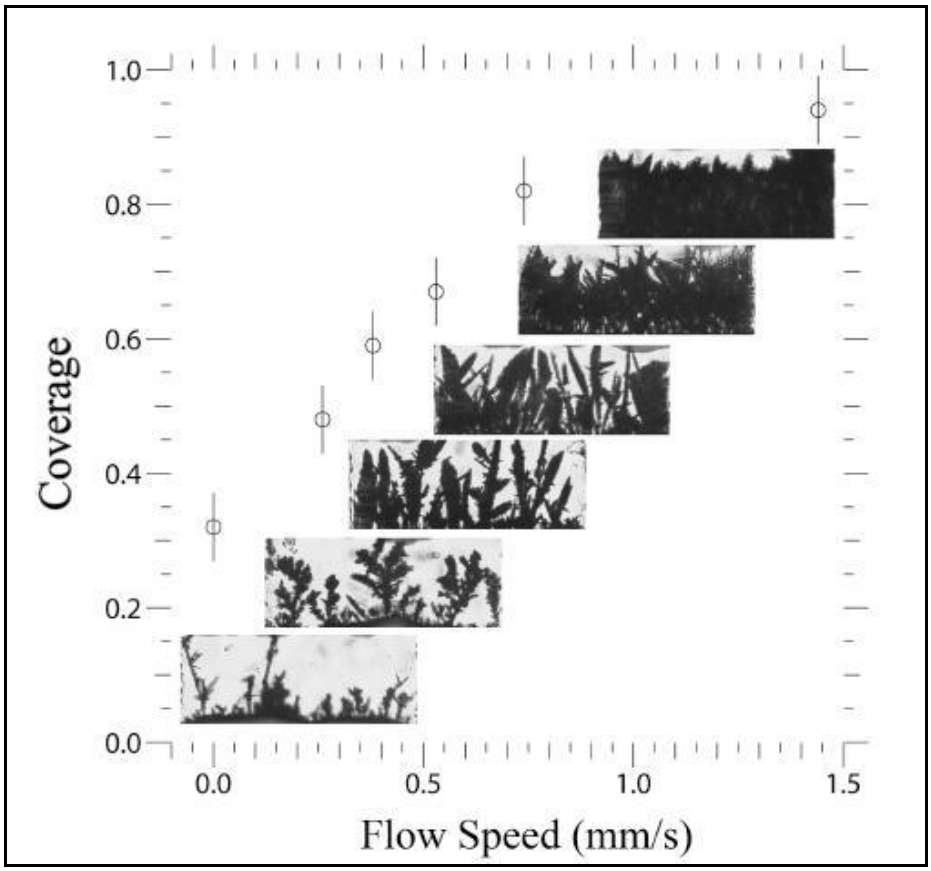

Figure 4.10 – Micrographs of area in electrodes gap [22]

4.5 Experimental data analysis

For having a sense of where and when connection in the gap between electrodes happens we analyze V_{out} vs. time graphs. Quantization data analysis about changes of voltage and measuring number of conductance as mentioned in chapter 3 are useful to consider in this part.

In our experiment, we defined in the LabView program that sampling rate to be 1 ms. This means in each 1 ms system records one data point. In graph, that shows relation between

V_{out} and time, each vertical point in V_{out} axis corresponds one data point in horizontal time axis. Frequency of data sampling is defined as below:

$$f = \frac{1}{\Delta t} \rightarrow f = \frac{1}{10^{-3} s} = 10^{3} Hz \qquad (4.1)$$

For mathematical analysis, in order to recover all Fourier components of a periodic waveform, it is necessary to use a sampling rate ν at least twice the highest waveform frequency .Nyquist frequency, also called the Nyquist limit, is the highest frequency that can be coded at a given sampling rate in order to be able to fully reconstruct the signal [26]:

$$f_{Nyquist} = \frac{1}{2}\nu \qquad (4.2)$$

So in our experiment Nyquist frequency is $f_{Nyquist} = 500 Hz$.

Figure 4.11 shows data recording from one of our samples (AAI-02), that we got by an Running the experiment at room temperature. The total time is about 320 s and the highest is $Y_{\max}(avg.)$ which is about 0.879 Volt. Because of noise during data gathering a sharp point in a short period of time for interval was not obvious and the peak point can be approximated by averaging the successive points. The maximum point in vertical axis, output voltage, is where the connection happens in the actual setup. After that system self terminates itself. A few movements of ions still continued until the steady state happens. But mentioning time and place of connection is important from this point of view that in captured videos we can find out exactly the actual place and reaction.

We did some noise analysis by using LabView, which will be explained in detail in next chapter. But before that some discussions about shape of the graph are important.

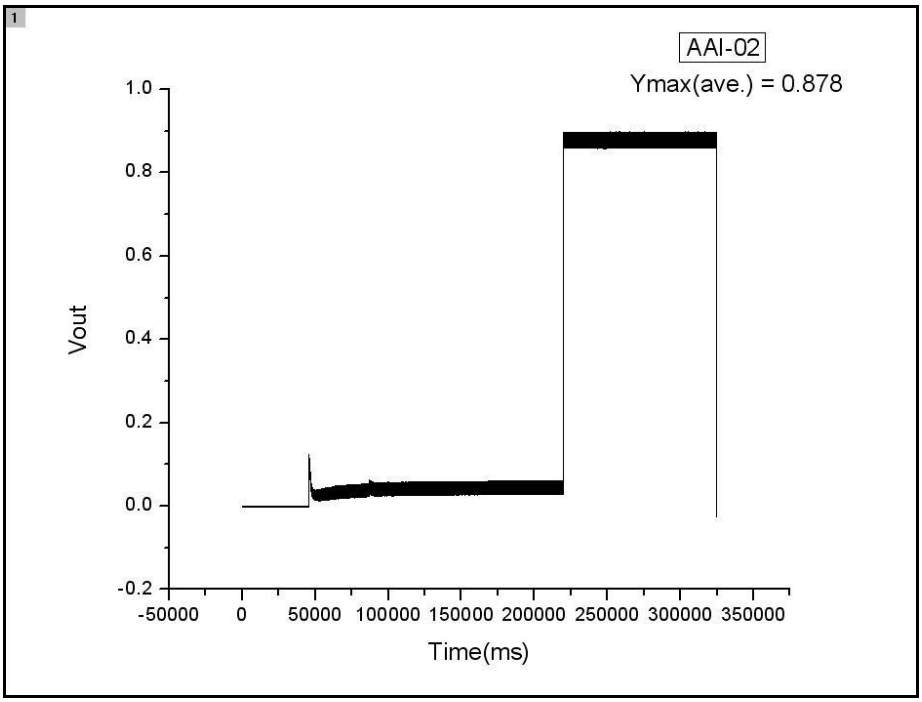

Figure 4.11 – Output voltage vs. time for AAI-02 sample

4.6 Electrochemical interoperation of peaks

In this section some discussions based on electrochemical reactions will be followed. Time scale and amplitude that these peaks happen are important parameters. Generally the maximum peak takes place when the connection happens and it is related to the movement of electrons.

Data gathering is started when bias potential turned on to 1 Volt. It takes about 50 ms (according to time scale of the graph 4.11) that ions set up in solution of electrode and electrolyte and in that time some oxidation and reduction processes happened inside system.

In our experiment some reactions are going on between ions of gold and HCl as electrolyte. And this happens locally between each electrode and solution around so without any flow inside the HCl and assuming a separation between electrodes, a current is flowing between

anode and cathode through the external circuit. As a result there is a local peak at the beginning in the graph which shows this process.

Back to graph, after this small peak a steady state happens that is a sign of open circuit. During this time by force of bias potential ions of gold move from cathode to anode through electrolyte of HCl and slightly accumulate on the other side. This makes other side electrode to be etched away.

To be accurate it can be said electrodeposition happens between electrodes and after a while pseudo tunnelling regime takes place and the big peak is the reason for that. Now the growth of connection between anode and cathode is completed, and the electro-deposition accumulation between electrodes becomes long enough to make a wire-like connection. By this bridging way electrons can move from one side to the other and current flows through it. This connection considers as a short circuit so electrons instead of passing external circuit prefer to move in this way which has lower resistance and this is the accomplishment of experiment.

When this is done system tries to self-terminate itself and when the rate of moving ions become slower and estimated to be stopped the current becomes zero so a big descend can be seen from the edge of short circuit.

An error region is clear in the whole process of experiment and it is because of noise that we figured out the ripple of it is 60 Hz. This frequency is close to frequency of AC line and it can be deleted by a big percent when we used Fourier filtering analysis.

4.7 Discussion on plotted data

As mentioned in details of experimental work, we defined sampling rate as 10^3 Hz. It is the frequency of data sampling, so distance between two data point in the graph is this number. One data point is representative of 1 ms.

4.7.1. Different trends in output voltage

There two trends mainly happen in the connection point. First one is jumping of output voltage from zero to about 0.8 Volt (in average) at connection point. The other one is a gradually increasing trend of voltage from zero to about 0.8 (in average). Figure 4.12 is showing the sudden jump trend.

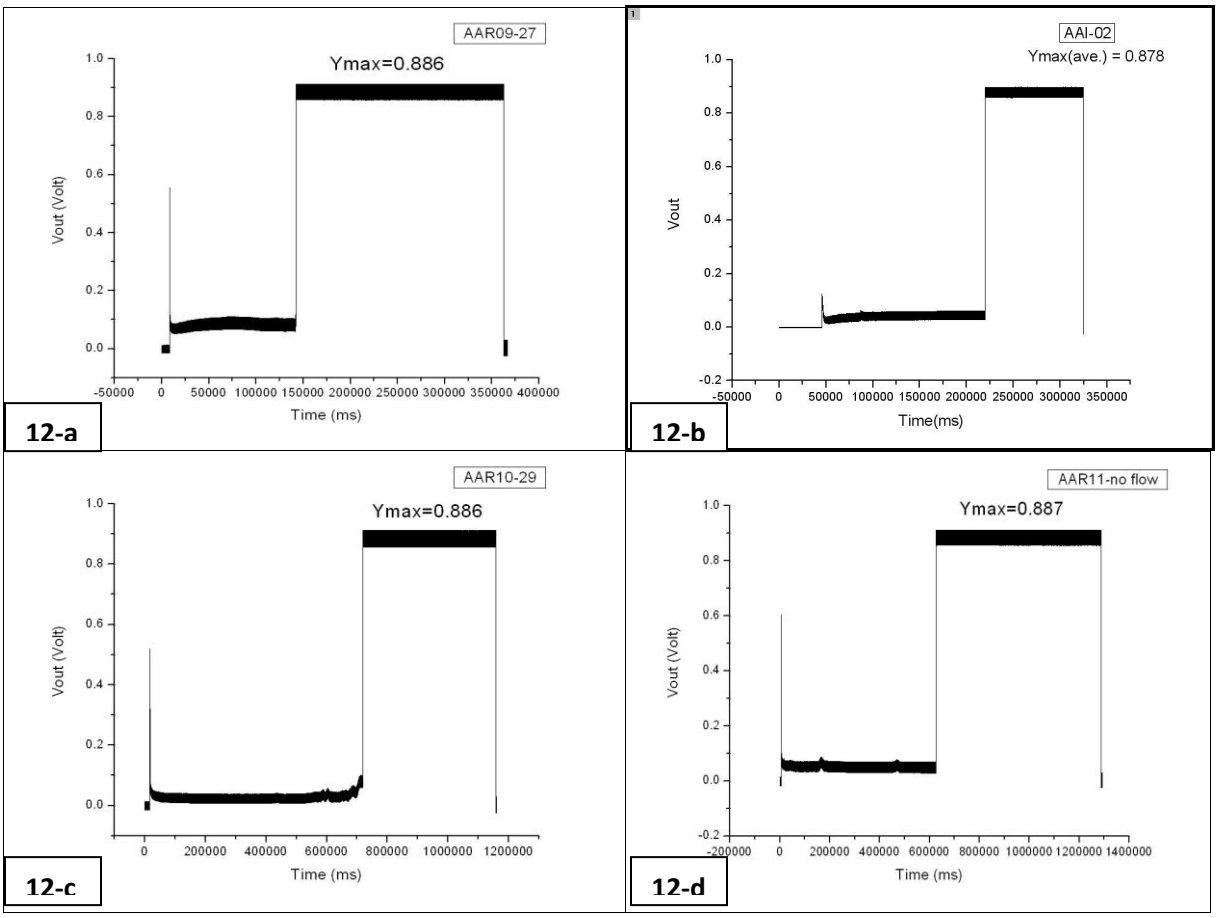

Fig. 4.12 Jump trend in Output voltage vs. time, fast to slow rate, (12-a): rate 27 (12-b): rate 28 (12-c): rate 29 (12-d): no flow

The second trend is showing in figure 13. Gradually increase in the voltage can be a sign of tunnelling regime of electrons in the gap of electrodes.

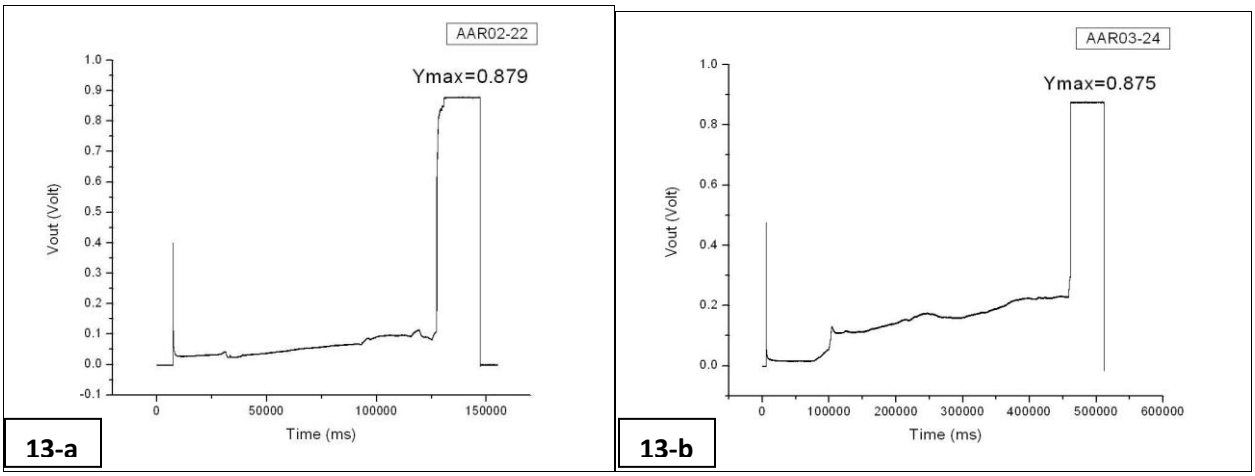

Fig. 4.13 Gradually increase trend in Output voltage vs. time, (13-a): rate 22 (13-b): rate 24

The gradually increasing trend is kind of step-shape raise of output voltage at connection point. Also two peaks that we discussed in previous section are obvious in all Vout-time graphs. First trends happened in majority of samples, but second one just has been showed up in a few of fabricated samples.

4.7.2. Different trends in conduction

The main concept that we should discuss as result of our experiment is to show that we get the real quantum point contact. Evidence for proving the idea, is to show if we get quantized conductance. In chapter 3 we showed calculations and data analysis for relating output voltage to conductance. So we got the results and plot number of conductance vs. time. In over than 100 experiments that we run, two main trends were obvious. One trend is obvious in figures below. It is showing a jump in conduction from zero to a constant multiple of quantum conductance. Because we have noise in data acquisition, specifying an exact number for conductance is

impossible. But in average it is between 2 – 4 multiples of G_0. This is the trend in majority of experiments.

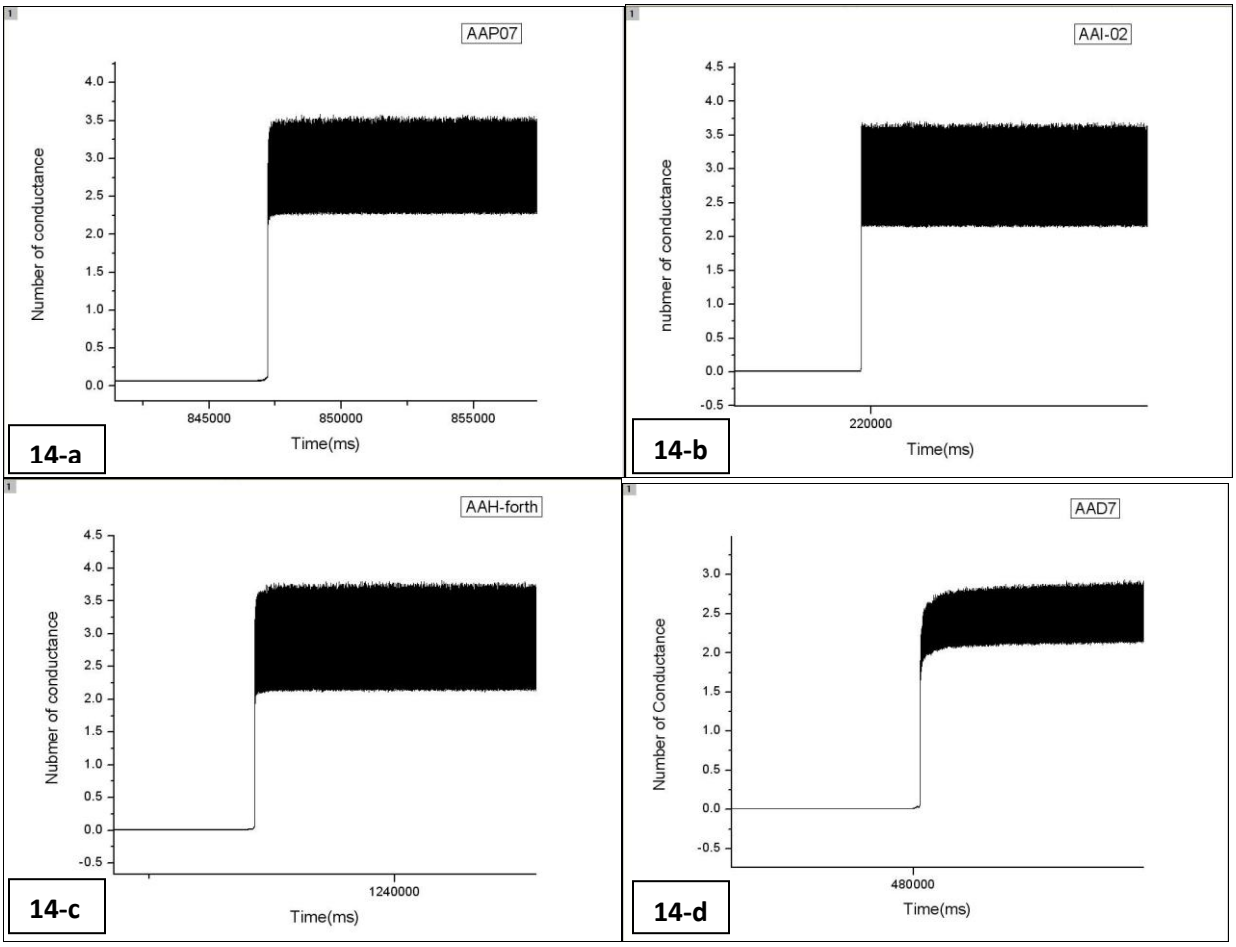

Fig. 4.14 – Jumping trend in quantum conductance – (14-a): rate 22 – (14-b): rate 28 – (14-c): rate 30 – (14-d): no flow

Figure 4.14 showing the mentioned trend in different samples. They are sorted from fast flow to slow flow and as it is obvious shape of conductance is not dependent on rate of flow. And the fact is conductance jumps to a multiple of G_0. There is no step shape raise in these graphs and current just flows from zero conductances to $2G_0 - 4G_0$.

Another trend which we expected and it happens in majority of experiments is step shape trend. We are looking for raise of conductance from zero to a constant number which is multiple of G_0. Some of these trends are showing in figure below.

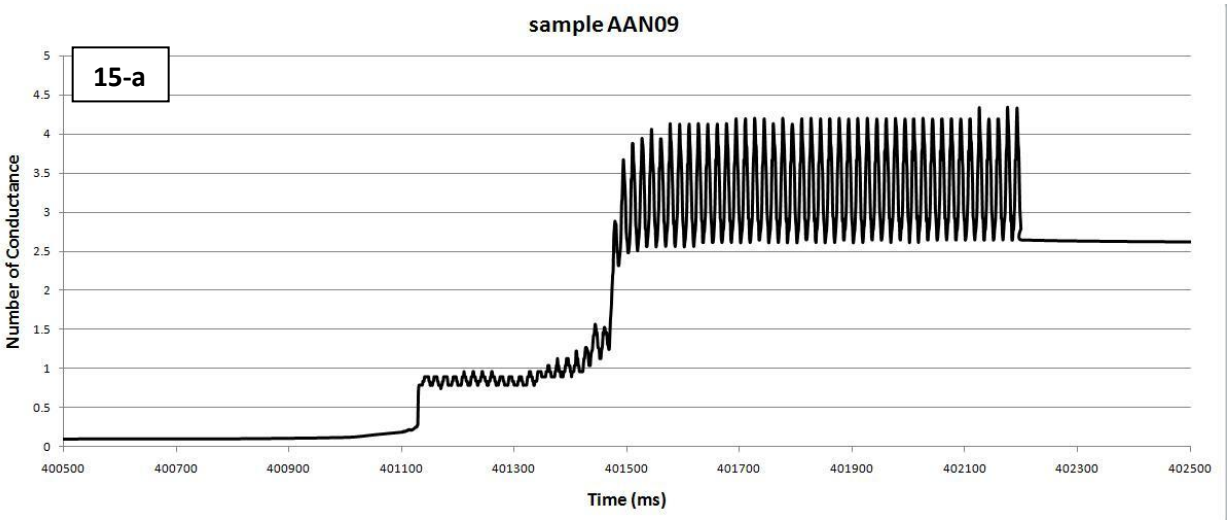

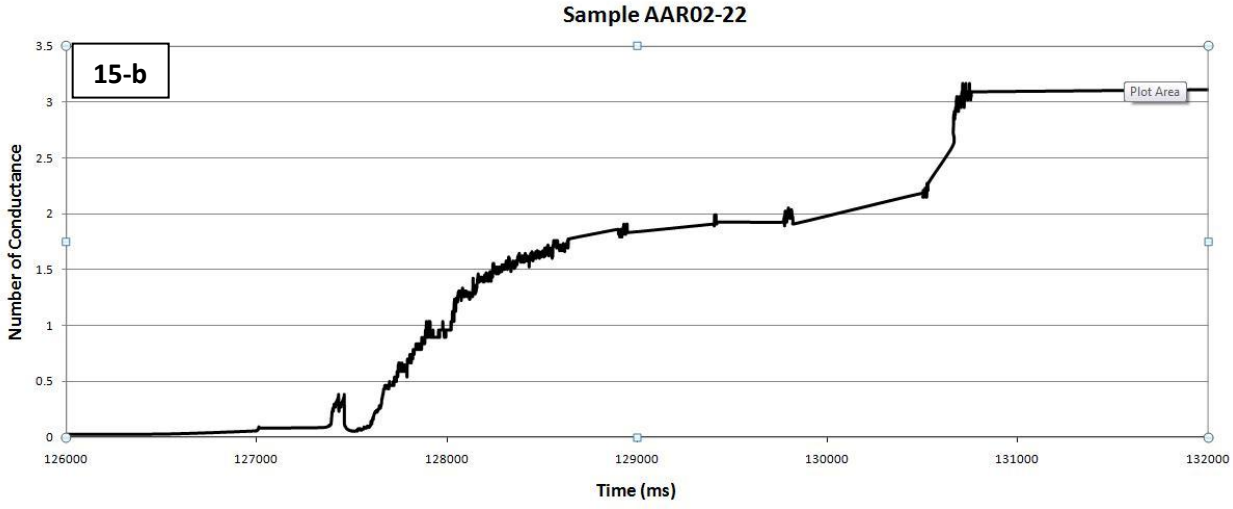

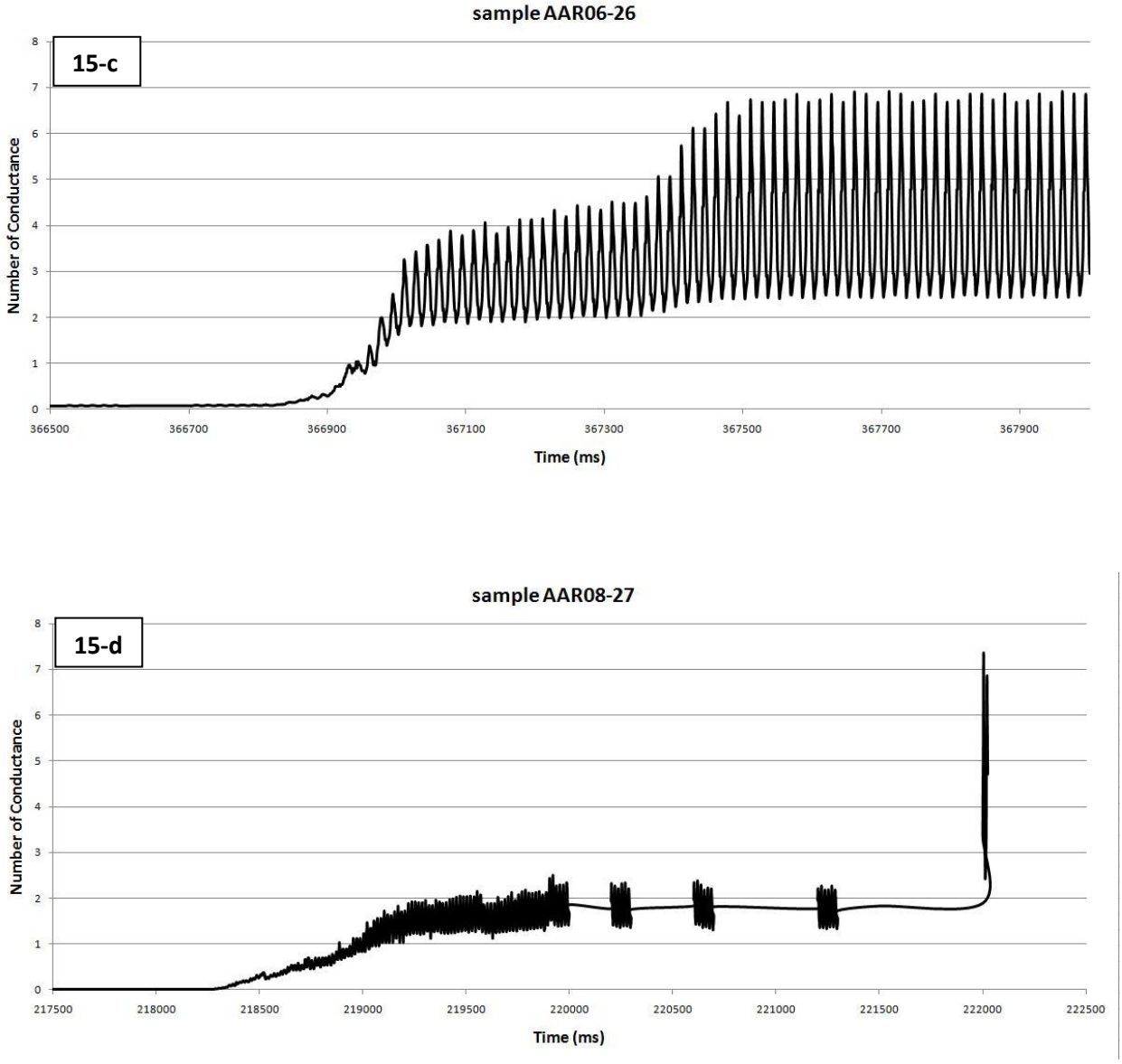

Fig. 4.15 – Step shape trend of quantum conductance – (15-a): rate 22 – (15-b): rate 22 – (15-c): rate 26 – (15-d): rate 27

Again this trend is independent of rate of flow. The step shape is observed but it has a tendency to pass from G_0 and reaches the higher multiples of G_0. The transition of conductance from zero to higher conductance is interesting in steps. One reason for having small steps is self

terminated system hasn't worked as we expected and stopped the growth is somewhere after first connection. So we were successful to make quantum point contacts but they last for a short period of time in one G_0 and then they become bigger in conductance multiples of G_0.

For example we zoomed in one of the step shaped samples above fig. (4.15-a) and it is showing the focused region. We are interested to show difference before and after connection and emphasis on time interval that we were successful to keep one G_0 conductance as quantum point contact.

It is showing the focused window of data in time interval from 401.100 s to 402.3 s. In this region the connection between the gap happens. Before 401.1 s the number of conductance is about zero. Electrons are moving in the gap space and may some of them can reach the other side electrode, but conductivity is very low and it is not in order of quantum conductance. The conductance is less than the quantum conductance. At 401.1 s there is a peak in the conduction and electrons can pass the connection. This means finally they reach the quantum of conductance. So we got the quantum point contact. This lasts until 401.5 s. For a period of 400 ms we could keep this quantum point contact. After this time because self termination process did not work out properly, fabrication continues to another rise in the graph as the second peak. This peak also shows conductance of quantum but it is multiple of quantum conductance. Because of unwanted noises there are ripples in the curve, so pointing out an exact number for conductance is not possible. By averaging it is between $2.5\,G_0$ or $4.5\,G_0$. More accurate data analysis for this part has been done in noise analysis part by filtering processes.

4.8 Experimental difficulties and error sources

Two main sources of errors can be discussed as electrical noise that can affect data analysis and problems of handling microfluidic channels.

4.8.1. Microfluidics: There are advantages and disadvantages in working with microfluidics channels. As an advantage, about guiding rule of these channels inside the electrodes to help ions find better direction, we talked before. Disadvantage of them mainly relates to difficulties of setting them up in the experiment.

The problem that we dealt with was leakage of channels. When we made channels in the PDMS chip and clamp it with gold slide and Plexiglas plates, the problem came out. Applying enough pressure to both end of clamping set up and fix enough space between gears of screws needs lots of trails and errors. If HCl leaks out of channel then we cannot talk about any special rate of flow in the channel. Because leaked flow will change the volume of electrolyte in the channel and rate of electrodeposition will be affected then.

For solving this problem we came up with plasma treating method. We put both gold slides and PDMS chip in the plasma treating system. After an appropriate time we put them on top of each other and this makes a good sealing. This lowers chance of leakage but depends to speed of flow sometimes worked well sometimes not. It solved problem to a good percent.

4.8.2. Noise: When we zoomed furthermore the frequency of noise is more obvious. In graph below some ripples look obvious which they are the sign of noises in the signal.

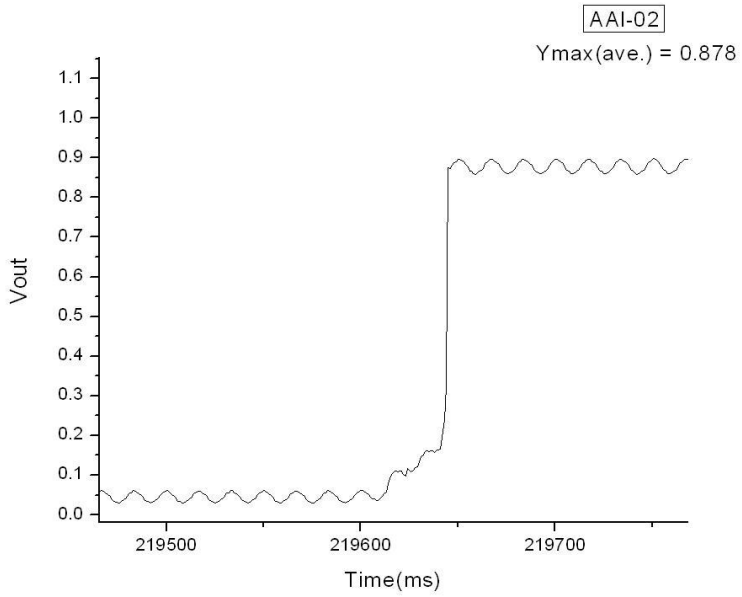

Figure 4.16 – Zoom in output voltage vs. time in sample AAI-02

When we zoomed in connection time at the point which is called connecting region, the frequency of noises is more obvious. By looking closer to signal we estimated that the time interval between two successive s of ripples is about 17 ms. This means, there are 17 points in a period which

$$f_{\exp} = \frac{1}{\Delta t} = \frac{1}{17ms} \approx 58.83Hz \cong 60Hz \qquad (4.5)$$

After comparing plotted data, it is clear that at what time the connection happens. This transition cannot happen suddenly and always there is a transition time between these two levels. Voltage cannot reach the maximum point suddenly and it increases gradually. Also it can be extracted from fig. 4.18, that some a very short time connection rises up like a step-wise form. As a reason to prove it and have a better view we need to avoid and delete unwanted noise. The

frequency of experimental noise has been known to be 60 Hz, so by using filters this can be ignored from actual signal. For this reason we should convert the time domain signal to frequency domain signal trough Fourier transform. Details of noise analysis are discussed in the appendix.

Now we found out that there is a 60 Hz noise signal in our data gathering. From the point this happens to be a usual noise in most electrical circuits and measurements, we decided to find out source of noise. One of main sources was signals that came from power supply. So by the help of electronic shop we changed assembly of power supply and connecting wires to our actual set up. As a result to very good extent the noise was deleted.

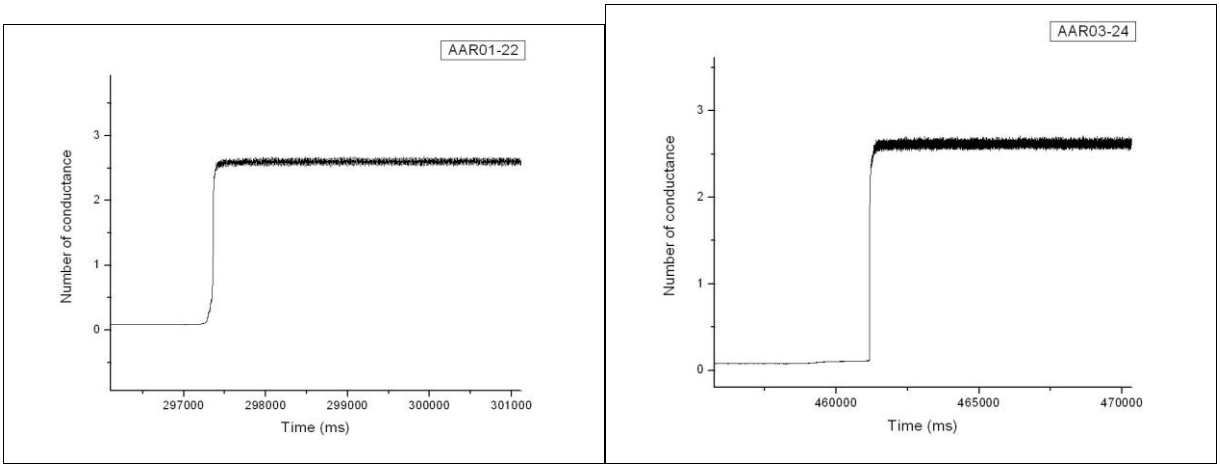

Fig. 4.17 Jumping trend in quantum conductance after deleting noise from power supply

We also did a filtering process with gathered data from some of experiments. Noise analysis has been done with LabView program. There is a following section describes whole process in detail.

4.9 Noise Analysis

For example in sample AAI-02 (Fig.14-b) the maximum voltage is 0.878 Volt and this is the point that connection happens. First and second peaks are also obvious in this sample. The total time takes about 320 s. It means we have 490000 acquired data points in the graph.

$$f = \frac{1}{\Delta t} = \frac{1}{320s} \approx 0.0031Hz \qquad (4.6)$$

This frequency has been defined as frequency step which in Fourier analysis is called resolution. It shows lower boundary of bandwidth frequency of data points in the experiment and $10^3\,Hz$ is upper band of this bandwidth.

0.0031 Hz < frequency of data points < 1000 Hz (4.7)

For showing a repeated period it is important to mention the first point in Fourier series is DC, so lower bandwidth frequency is zero. For avoiding repeating data acquisition twice in each period Nyquist frequency has been used which is half of upper band frequency. In a period bandwidth frequency is:

Zero < frequency of data points < 500 Hz (4.8)

By comparing figures 14 and 15 it is clear when the connection happens. After that time we have short circuit and before it we have open circuit. But as it showed this transition cannot happen suddenly and always there is a transition time between these two levels. Also it can be extracted from figures that in a very short time connection rise up in step-wise form. For prove it and have a better view we need to avoid unwanted noises.

The frequency of experimental noise has been known to be 60 Hz, so by using filters this can be ignored from actual signal. For this reason we first should convert the time domain signal to frequency domain signal trough Fourier transform. More detail has been provided in the appendix.

LabView is a helpful package which makes it very easy just to find necessary tools and connect them. Input is raw data that we get from experimental set up as V-out vs. time , then by using the formula that mentioned in chapter 3 for finding conductance , we get number of conductance data, and then we send all this to filter tool which automatically is doing FFT and result is filtered data.

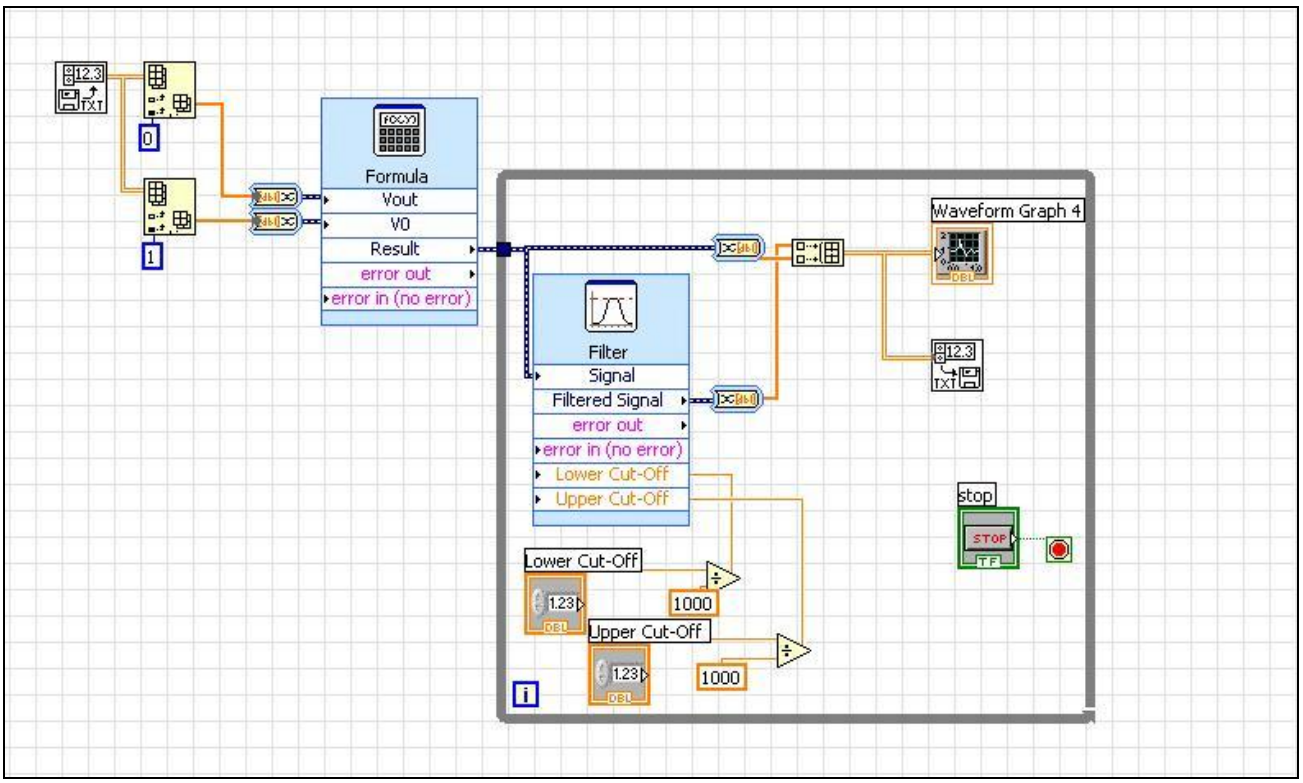

Figure 4.18 – Filtering data by band-pass filter (Upper cut-off: 0.08, Lower cut-off: 0.04)

For finding out which kind of 1/f noise we get here, we came up to this point that filtering two portion of our signal individually will give us the idea of dependence of signal to order of frequency. For this purpose we extracted part of signal before connection and part of signal after connection and this will give us a perfect view of shape of line.

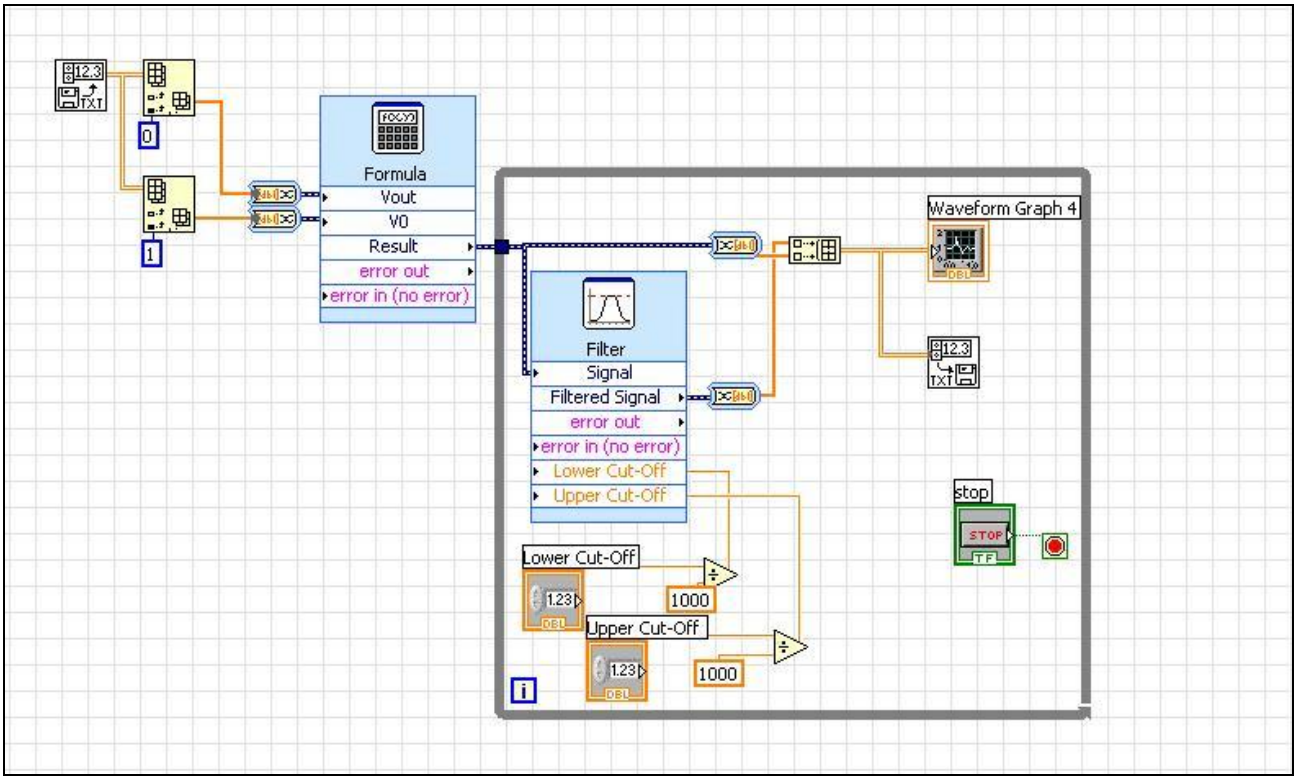

Figure 4.19 – Extracting portion of signal and filtering

By comparing results of filtering of two mentioned portion we found out that both side has linear shape, so order of dependence to frequency is one. This indicates that we get white noise in our experiment.

4.10 Suggestions for future work

Changing some of the conditions of experiment will help to get better results. As we compared related works with our recent data, decreasing the gap distance from 100 μm to about 20 μm will make big changes in shape of growth to fabricate quantum shaped tips.

Having lower concentration (2M → 0.2 M) will cause obvious change in electrochemical rate. Local concentration of ions varies in the point contact by this change and as a result conducting nanowires turns out to be a quantum point contact.

If we change bias voltage from 1V to 0.8V ions will have more time to find their direction so more regular shape of growth is expected.

In a macroscopic view self-terminated process and nano wires between micron sized gaps can be simulated by a bigger model in electrical circuits. The closest device is an antifuse. It performs the opposite function to a fuse. Whereas a fuse starts with a low resistance and is designed to permanently break on electrically conductive path (typically when the current through the path exceeds a specified limit). An antifuse starts with a high resistance and is designed to permanently create an electrically conductive path (typically when the voltage across the antifuse exceeds a certain level). This technology has many advances in IC-design and some other ongoing research.

The antifuse method closes the circuit by "growing" a conductive via. Two metal layers sandwich a layer of non-conductive, amorphous silicon. When voltage is applied to this middle layer, the amorphous silicon is turned into polysilicon, which is conductive.

In Fig 4.22 a schematic view of antifuse is observable. Two metal layers can be estimated to our two gold electrodes and non-conducting crystalline looks like isolating gap in our experiment.

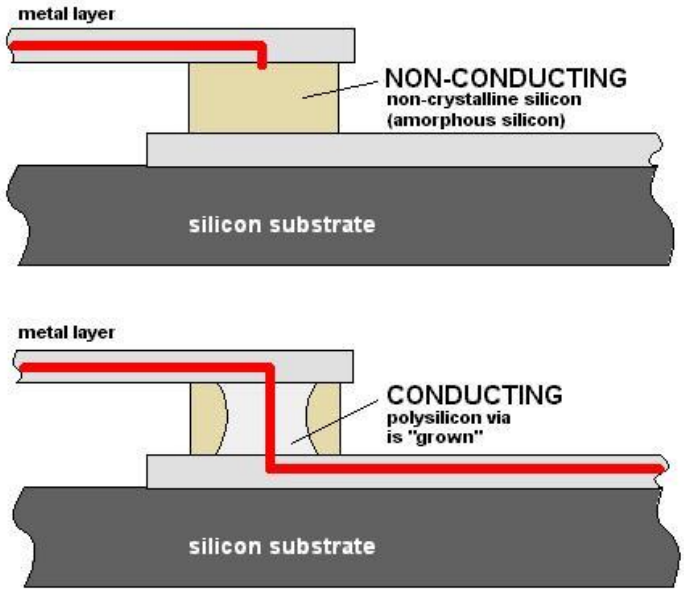

Figure 4.20 - Antifuse

In the experiment developed in our research, pressure – driven flow is applied during the deposition process in the anode to cathode direction in an effort to influence ion transport. The etching takes place all over the anode surface, but the dissolved metal ions are guided by the electric field and direction of HCl flow. By controlling these parameters, furthermore the electrochemical fabrication approach the rate of reaction and growth is controllable and this introduces large variance in the formation and location of individual junctions. It would be helpful to make a desired nano wire and a quantum point contact. Understanding and controlling

this process will enable the precise positioning of reproducible geometries into nano – electronic devices.

Bibliography

[1] G. Deutscher and R. Maynard; "From the Andreev Reflection to the Sharvin Contact Conductance"; NATO Science Series: B; Kluwer Academic Publishers; MA; USA; 2006

[2] Henk van Houten and Carlo Beenakker, "Quantum Point Contacts", Physics Today, page 22, July 1996

[3] Hideki Hasegava, "Advanced mesoscopic device concepts and technology", microelectronic engineering 53, 29 -36 (2009)

[4] Siegmar Roth, David Carroll; "One-dimensional metals: conjugated polymers, organic crystals, carbon nanotubes", Wiley-VCH; 2004 ; http://media.wiley.com/product_data/excerpt/94/35273074/3527307494.pdf

[5] H.X. He and S. Boussaad; "Electrochemical fabrication of atomically thin metallic wires and electrodes separated with molecular-scale gaps"; Journal of Electro analytical Chemistry 522, 167-172 (2002)

[6] R. de Picciotto, H. L. Stormer, L. N. Pfeiffer, K. W. Baldwin& K. W. West; “Four-terminal resistance of a ballistic quantum wire”, Nature 411, 51-54, May 2001

[7] Andr´as HALBRITTER, “Investigation of atomic-sized conductors with the mechanically controllable break junction technique”, PhD Thesis, Budapest University of Technology, Department of Physics (2003)

[8] Samuel Glasstone; “An Introduction to Electrochemistry”, Ninth edition, D. Van Nostrand Company Inc., Princeton, New Jersey, 1942

[9] Hiroyuki Ohno, “Electrochemical Aspects of Ionic Liquids”, John Wiley and Sons Inc., New Jersey, 2005

[10] T. Kita1, T. Kakegawa, M. Akabori and S. Yamada, “Spin-polarized transport in adiabatic quantum point contact with strong Rashba spin–orbit interaction”, Solid State Communications 136, 479–483 (2005)

[11] Richard A. Webb and Sean Washburn, “Quantum interference fluctuations in disordered metals”, Physics Today, Dec 1988

[12] T. Giamarchi; “Umklapp process and resistivity in one-dimensional fermion systems”; Physical Review B, 44 (7), Aug. 1991

[13] S. K. Lyo and Danhong Huang , “Effect of electron-electron scattering on the conductance of a quantum wire studied with the Boltzmann transport equation”, Physical Review B , 73 (20) , (2006)

[14] Chris Winstead, “Mobile carriers and the Fermi function”; Connexions sponsored by Rice University; Feb 2006; http://cnx.org/content/m13458/latest/

[15] B.J. van Wees, Department of Applied Physics, Delft University of Technology; Netherlands; 1989; http://www.weizmann.ac.il/condmat/imry/images/nano.html

[16] Supriyo Datta; “Electronic transport in mesoscopic systems”; Cambridge studies in semiconductor Physics and microelectronic engineering, page 52, 1995

[17] B. J. van Wees and H. van Houten; “Quantized conductance of point contacts in a two-dimensional electron gas”; Physics Review Letters 60 (9), Feb. 1988

[18] S. Boussaad and N. J. Tao; “Atom-size gaps and contacts between electrodes fabricated with a self-terminated electrochemical method”; Applied Physics Letters; 80 (13), April 2002

[19] Michael S. Fuhrer; Department of Physics; University of Maryland at Colledge Park; http://www.physics.umd.edu/mfuhrer/molresearch.htm

[20] C. Z. Li and N. J. Tao; "Quantum transport in metallic nanowires fabricated by electrochemical deposition/ dissolution"; Appl. Phys. Lett. Vol. 72, Num. 8, Feb. 1998

[21] Michael Schmid, Department of Physics; IAP/TU Wien
http://www.iap.tuwien.ac.at/www/surface/STM_Gallery/stm_schematic.html

[22] A. Wlasenko, F. Soltani, D. Zakopcan, D. Sinton, and G. M. Steeves, "Diffusion−Limited and Advection−Driven electro deposition in a Microfluidic Channel"; Phys. Rev. E 81, 021601 (2010).

[23] Atkins, P.W., "Physical Chemistry", W. H. Freeman and company, San Francisco, (1983) 1042-1049

[24] A. Bogozi, O. Lam, H.X. He, C.Z. Li, N.J. Tao, L.A. Nagahara, I. Amlani, R. Tsui, J. Am. Chem. Soc. 123 (2001) 4585.

[25] MicroChem Corp, "NANOTM SU-8 Negative Tone Photo resists Formulations 50-100", Data sheets, 2001

[26] David Irwin; "Basic engineering circuit analysis"; 6th edition; Wiley; 1994

[27] C. Gasquet, P. Witomski; "Fourier analysis and Applications"; Springer; New York; 1998

[28]Don Johnson; “Fourier Series Approximation of Signals”; Connextions sponsored by Rice University; Jun 2009; http://cnx.org/content/m10687/latest/

[29] Eric W. Weisstein, "Fourier Series--Square Wave."; MathWorld; Wolfram Web Resource.

http://mathworld.wolfram.com/FourierSeriesSquareWave.html

[30] NI Developer Zone; “Using Fast Fourier Transforms and Power Spectra in LabView” ; National Instruments; Sep 2006; http://zone.ni.com/devzone/cda/tut/p/id/4541

[31] Richard G. Lyons; “Understanding Digital Signal Processing”; Prentice Hall; New Jersey;

2004

[32] Brian Jones; “Circuit electronics for scientists”; Addison-Wesley publishing company;

London; 1974

[8] M. J. Buckingham; “Noise in electronic devices and systems”; Ellis Horwood Limited;

London; 1983

[34] Stefan Niewiadomski; “Filter handbook, a practical design guide”; Heinemann Newnes;

Oxford UK; 1989

[35] S. Roy Morrison, “Electrochemistry at semiconductor and oxidized metal electrodes”, Plenum press, New York, 1980

Appendix

Noise determination and methods

If we want to have a well defined view of signals, first we should go for some good definitions. The observation of some phenomenon yields certain quantities that depend on time (on space, on frequency or etc.). These quantities, which are assumed to be measurable, will be called signals. They correspond in mathematics to the notion of function and some variables, and thus signals are modeled by functions. In our experiment, we tried to record changes of current by growing the connection in the gap between electrodes when time is going on. As a result, we got a curve that shows relation between current and time. There are ripples in the graph which are from noise

sources. Noise analysis is described in this chapter to delete defects and results from actual data are more obvious.

General considerations in Fourier analysis

1. Periodic functions: As $f(t) = f(t + nT)$ are useful to express Fourier demonstration and in our data processing it will be showed as sum of sinusoidal functions. The term signal processing refers to analyze time varying processes. An analog type signal used to describe a waveform that's continuous in time and can take on a continuous range of amplitude values. Analog signals can be applied to a conventional spectrum analyzer to determine their frequency content. Another relevant type is digital signal processing (DSP) which more deals with discrete-time or pulsed shape signals. Here we mostly characterize the frequency content of continuous time domain signals.

The continuous Fourier transform $X(f)$ defined as

$$F\{x(t)\} = X(f) = \int_{-\infty}^{\infty} x(t)e^{-j2\pi ft}dt \qquad \text{(A.1)}$$

where $x(t)$ is some continuous time-domain signal.

This equation is used to transform a continuous time-domain function $x(t)$ into a continuous frequency-domain function $X(f)$.

2. DFT: The discrete Fourier transform (DFT) enables us to analyze signals very well. It is a mathematical procedure used to determine frequency content of a discrete signal sequence. It used to call Fourier series analysis. For discrete frequency-domain sequence $X(m)$, DFT is defined by this equation

$$X(m) = \sum_{n=0}^{N-1} x(n) e^{-j2\pi mn} / N \qquad \text{(A.2)}$$

where $x(n)$ is a discrete sequence of time-domain sampled values of continuous variable $x(t)$. [27]

It has been proved that if a periodic function is expressed as sum of linearly independent functions, each function in the summation must be periodic with the same period.

For example Fourier series approximation for a square wave can be shown by adding different series together and observing the estimated result in each time. Total wave form tries to be close as possible to a square wave. More number of series makes approximation much more accurate and it become closer to square wave shape.[28],[29]

Square wave function: $f(x) = \frac{4}{\pi} \sum_{N=1,3,5,\ldots}^{\infty} \frac{1}{N} \sin(\frac{N\pi x}{L})$ (A.3)

where N is number of series and 2L is length of a period.

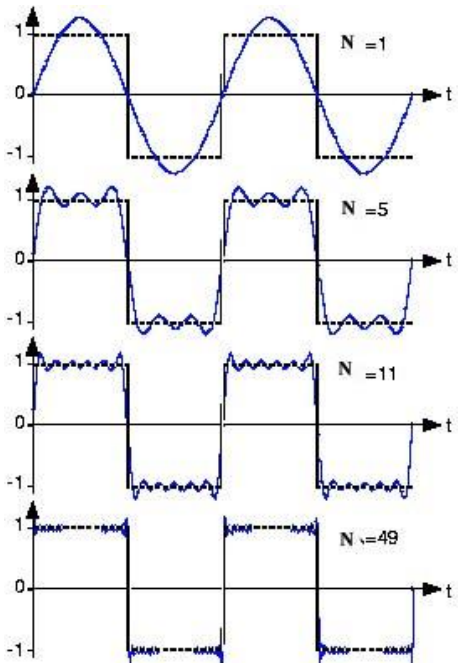

Figure A.1- Fourier series [28]

That can be shown in a final estimation of:

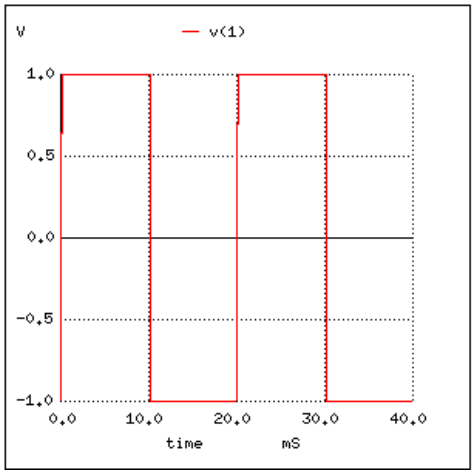

Figure A.2 – Square wave [29]

3. FFT: Fast Fourier transform (FFT) computes the DFT and produces exactly the same result as evaluating the DFT. The only difference is that an FFT algorithm is much faster than evaluating

the DFT definition directly. FFT is a powerful signal analysis tool, applicable to a wide variety of fields including spectral analysis and digital filtering [31].

From Euler's relation $e^{-j\theta} = \cos(\theta) - j\sin(\theta)$, relation for discrete frequency domain sequence is equivalent to

$$X(m) = \sum_{n=0}^{N-1} x(n)[\cos(2\pi mn / N) - j\sin(2\pi mn / N)] \qquad \text{(A.4)}$$

which is in rectangular form and complex exponential has been separated into its real and imaginary components. where

$X(m) =$ the m th DFT output component, i.e., $X(0), X(1), X(2), X(3),$ etc.

$m =$ the index of the DFT output in the frequency domain

$m = 0,1,2,3,..., N-1$

$x(n) =$ the sequence of input samples, $x(0), x(1), x(2), x(3),$ etc.

$n =$ the time-domain index of the input samples, $n = 0,1,2,3,..., N-1$

$N =$ the number of samples of the input sequence and the number of frequency points in the DFT output.

Each $X(m)$ of DFT output term is the sum of the point for point product between an input sequence of signal values and a complex sinusoid of the form $\cos(\theta) - j\sin(\theta)$. The exact frequencies of the different sinusoids depend on both the sampling rate f_s at which the original signal was sampled, and the number of samples N.

4. Polar coordinate: Quiet often we're interested in both the magnitude and the power (magnitude squared) contained in each $X(m)$ term, and the standard definitions depicted in figure below:

Figure A.3 – polar coordinate

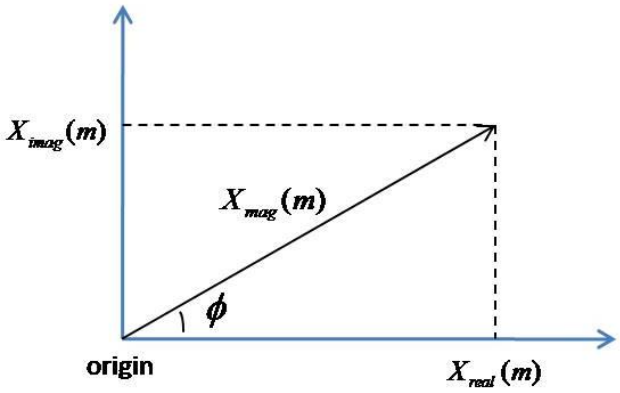

$$X(m) = X_{real}(m) + jX_{imag}(m)$$

$$X_{mag}(m) = |X(m)| = \sqrt{X_{real}(m)^2 + X_{imag}(m)^2}$$

$$X_{ps}(m) = X_{mag}(m)^2 = X_{real}(m)^2 + X_{imag}(m)^2$$

Data Analysis and using LabView

LabView and its analysis VI library provide a complete set of tools to perform Fourier and spectral analysis. The Fast Fourier transforms (FFT) and power spectrum VIs is optimized and their outputs adhere to the standard DSP format.

FFT and spectral analysis are performed only on real-valued, discrete-time sequences. The time-domain signal has a signal of interest buried in the noise that can be identified in the frequency domain. Based on frequency information, digital filtering can remove the noise from

the signal. In standard output format of LabView, for graphically display the results of FFT, output array is complex and requires two graphs to show all information [30].

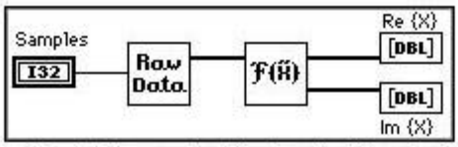

Figure 4. Block Diagram to Display the Standard Output

The real and imaginary portion of FFT VI results respectively are shown in two graphs below. The fact that they are symmetric is noticeable.

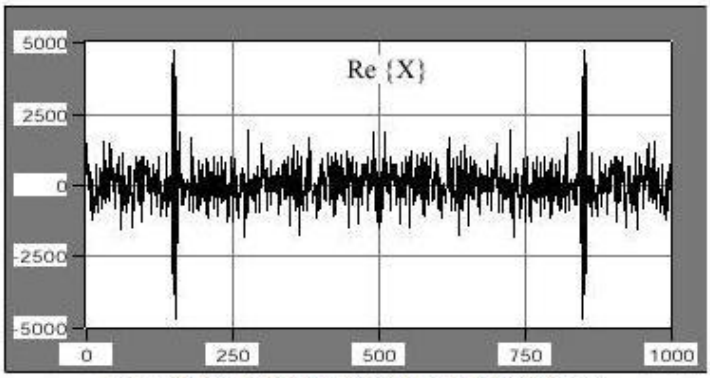

Figure 5. Real Portion of the Fourier Transform

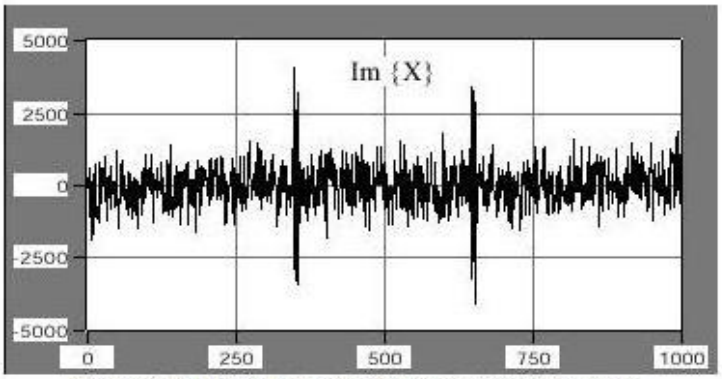

Figure 6. Imaginary Portion of the Fourier Transform

The power spectrum VI calculates the harmonic power in discrete-time, real-valued sequences. It is closely related to the FFT, to calculate the harmonic power in a signal.

It is defined by using the following equation:

$$S_{XX}(f) = X(f)X^*(f) = |X(f)|^2 \qquad \text{(A.5)}$$

where $X(f) = F\{x(t)\}$ and $X^*(f)$ is the complex conjugate of $X(f)$.

Unlike the FFT, power spectrum results are always real. The power spectrum VI runs faster than the FFT VI because it performs the computation in place and does not need to allocate memory to accommodate complex results [30].

Noise analysis

Noise in the broadest sense, can be defined as any unwanted disturbance that obscures or interferes with a desired signal. In most circuits, however, the unwanted signal is completely unrelated to any applied signal. Often the highest possible accuracy is needed in the measurement and processing of signals. This is especially important when you deal with accurate and small amplitude signals. As the sensitivity increases, a point will be reached at which unwanted signals, or noise, will obscure the required signal. In general, these noise signals will be grouped into three basic categories.

1. Avoidable signals can, in principle, be eliminated by more careful circuit design and construction. These signals include those derived from the power supply, other parts of the circuit and other electrical systems either near or far away. The signals originating outside the circuit can be reduced if contacts or from temperature changes.

2. Perhaps avoidable signals come from the particular properties of circuit and devices used. The source of these signals is therefore not inherent, but the devices and components that can be

obtained may not be ideal so that this source of noise can only be reduced by a major redesign of the circuit or by using better circuit elements when they are obtainable. For example, all amplifiers introduce noise signals and a given circuit may be improved by the purchase of a better and more expensive amplifying device, but at any time there is a "best" amplifying device so that the circuit is using this amplifier can only be improved by changes at some other point in the circuit or a major change in the type of circuit.

3. Unavoidable signals are due to the inherent statistical properties of nature. For a classical system, the noise is described by the equipartition theorem which states that for a system at a temperature T, each degree of freedom has $kT/2$ average energy. In some systems, the noise may be determined by discreteness of the electrical charge or by the quantized energy levels. This noise can only be reduced by a suitable choice of the experiment. [32] The three most commonly encountered types of unavoidable noises are thermal noise, shot noise and $1/f$ noise.

Thermal noise (or Johnson noise) arises from the random velocity fluctuations of the charge carriers (electrons and/or holes) in a resistive material. The mechanism is sometimes said to be Brownian motion of the charge carriers due to the thermal energy in the material. Thermal noise is present when the resistive element is in thermal equilibrium with its surroundings.

Shot noise is associated with the passage of current across a barrier, and in this sense is a non-equilibrium form of noise. It is frequently encountered in solid state devices, whenever a net current flows across a potential barrier such as the depletion layer of a p-n junction.

$1/f$ **noise** occurs in a wide variety of systems (electronic, biological, music, etc.), but particularly in solid-state devices, has come to achieve a certain notoriety. Historically it is also known as current noise, flicker noise, contact noise or excess noise. It shows a power spectral density which varies with frequency as $|f|^{-\alpha}$, where alpha usually falls between 0.8 and 1.4. This dependence has been observed down to frequencies as low as 10^{-6} Hz. The upper limit of its existence is difficult to establish because it is usually masked by thermal noise or some other type of noise. [8]

We are more focused here on $1/f$ noise, because it is the more probable noise that can be observed in our experiment. When a constant voltage (bias voltage) is applied across a resistor, a fluctuating component is observed in the current in addition to the thermal noise which is also present. This excess noise component that is observed in the presence of a DC voltage, as mentioned above show a power spectral density which varies as $|f|^{-\alpha}$, where alpha is more or less constant.

Spectral density (power distribution in the frequency spectrum) is such a property, which can be used to distinguish different types of $1/f$ noise. This classification by spectral density is given "color" terminology, with different types named after different colors. Many of these definitions assume a signal with components at all frequencies, with a power spectral density per unit of bandwidth proportional to $\frac{1}{f^{\alpha}}$ and hence they are examples of power-law noise. For instance, the spectral density of white noise is flat (alpha=0), while pink noise has alpha=1 and brown noise has alpha=2.

Filters

A filter is an electrical network which has some of its transfer characteristics frequency-dependent. Filters are used to change the frequency characteristics of signals by either attenuating or emphasizing some frequencies more than others. In this way a desirable signal can be extracted from a mixture of signals at other frequencies or a particularly undesirable frequency can be suppressed. The first step in becoming familiar with digital filters is to learn to speak the language used in filter business. The best known frequency-dependent characteristic of a filter is the input-to-output amplitude response.

1. Attenuation is an amplitude loss, usually measured in dB, incurred by a signal after passing through a digital filter. Filter attenuation is the ration, at a given frequency, of the signal amplitude at the output of the filter divided by the signal amplitude at the input of the filter, defined as

$$attenuation = 20.\log_{10}(\frac{a_{out}}{a_{in}})dB \qquad \text{(A.6)}$$

for a given frequency, if the output amplitude of the filter is smaller than the input amplitude, the ratio in equation above is less than one, and the attenuation is a negative number.

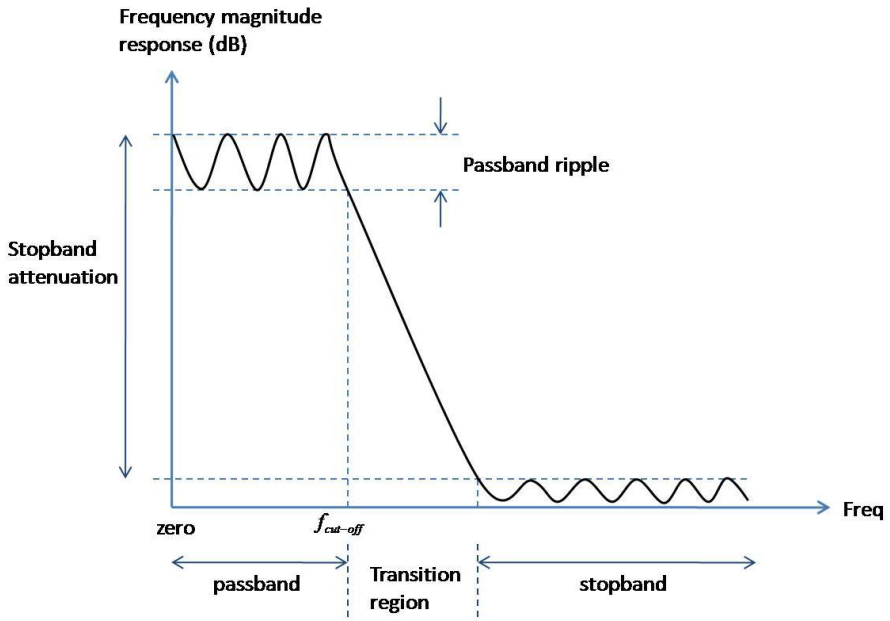

Figure A.7 – Parameters of noise

2. Passband is the frequency range over which a filter passes signal energy with minimum attenuation. Usually defined as the frequency range where the magnitude response is within the peak-peak passband ripple region.

3. Stopband is band of frequencies attenuated by a digital filter.

4. Ripple refers to fluctuations (measured in dB) in the passband, or stopband of a filter's frequency-response curve. Ripples in the stopband response are sometimes called out-of-band ripple.

5. Low-pass filter is a filter that passes low frequencies and attenuates high frequencies. Its passband extends from zero to some fixed frequency limit f_1 and its stopband extends from f_2 to infinity ($f_2 > f_1$).

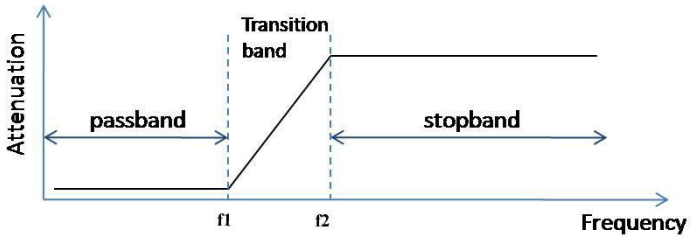

Figure A.8 – Low-pass filter

6. High-pass filter is a filter that passes high frequencies and attenuates low frequencies. It is a component of low-pass filter; i.e. the stopband encompasses the low frequencies and the passband the high frequencies beginning at f_1 .

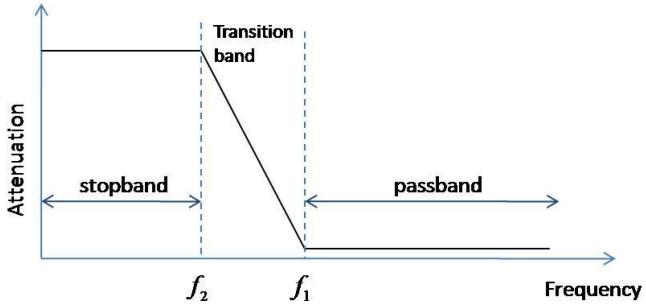

Figure A.9 – High-pass filter

7. Band-pass filter is a filter that passes one frequency band and attenuates frequencies above and below that band. Its stopband includes both high and low frequencies and contains a passband between the two finite frequencies f_1 and f_2.

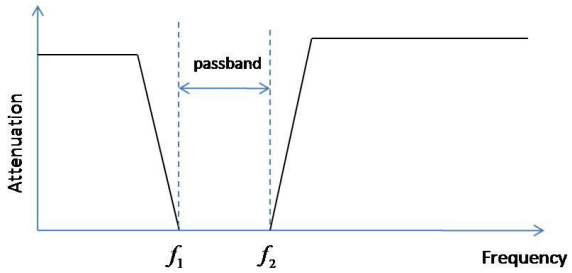

Figure A.10 – Band-pass filter

8. Band-stop filter (Notch filter) is a filter that rejects (attenuates) one frequency band and passes both a lower and a higher frequency band. It contains passbands on both sides of a stopband. The two passband edge frequencies are designed as f_1 , f_2.

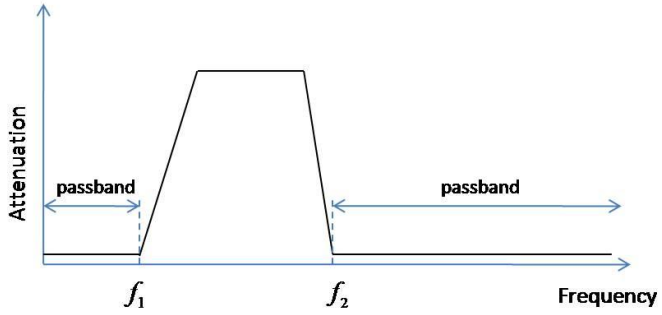

Figure A.11 – Band-stop filter

9. Cut off frequency is the highest passband frequency for low-pass filters (and the lower passband frequency for high-pass filters) where the magnitude response is within the peak-peak passband ripple region.

10. Bandwidth is the frequency width of the passband of a filter. For a low-pass filter, the bandwidth is equal to the cutoff frequency. For a band-pass filter, the bandwidth is typically defined as the frequency difference between the upper and lower frequency points [31], [34].

There are two main methods to use filters, first design electrical elements in a circuit to work as filter and second use filtering software which has been written to apply DSP methods on signals and omit noises as efficient as possible. By this way digital filter is a computational process, or algorithm, transforming a discrete sequence of numbers (the input) into another discrete sequence of numbers (the output) having a modified frequency-domain spectrum. Here we use later method and by applying LabView filter component and furrier analysis to signals, then we can get better results as expected.